UNIVERSITY OF CINCINNATI

Date: 05/04/2009

I, Sathyakumar S Kuntaegowdanahalli **,**

hereby submit this original work as part of the requirements for the degree of:

Master of Science

in Electrical and Computer Engineering

It is entitled:

Inertial microfluidics for continuous particle separation in spiral microchannels

Student Signature: Sathyakumar S Kuntaegowdan

This work and its defense approved by:

Committee Chair: Dr. Ian Papautsky

Dr. Jason Heikenfeld

Dr. Fred R. Beyette Jr.

Approval of the electronic document:

I have reviewed the Thesis/Dissertation in its final electronic format and certify that it is an accurate copy of the document reviewed and approved by the committee.

Committee Chair signature: Dr. Ian Papautsky

INERTIAL MICROFLUIDICS FOR CONTINUOUS PARTICLE SEPARATION IN SPIRAL MICROCHANNELS

A thesis submitted to the
Division of Research and Advanced Studies
of the University of Cincinnati
in partial fulfillment of the requirements for the degree of

MASTER OF SCIENCE

in the Department of Electrical and Computer Engineering
of the College of Engineering

2009

By

Sathyakumar Srinidhi Kuntaegowdanahalli

B.E. (Hons) Birla Institute of Technology and Science, India, 2005

Committee Chair: Ian Papautsky, Ph.D.

ABSTRACT

This work describes the use of inertial microfluidics for continuous multi-particle separation in simple spiral microchannels. The dominant inertial forces coupled with the Dean rotational force due to the spiral microchannel geometry cause particles to occupy a single equilibrium position near the inner microchannel wall. The position at which particles equilibrate is dependent on the ratio of the inertial lift to the Dean drag. Using this concept, a spiral lab-on-a-chip (LOC) design was demonstrated for the first time for focusing particles at distinct equilibrium positions in the microchannel cross-section based on size. The individual streams can be collected with an appropriately designed outlet system. To demonstrate this principle experimentally, a 5-loop Archimedean spiral microchannel with a fixed width of 500 μm and a height of 130 μm was used to simultaneously and continuously separate 10 μm, 15 μm, and 20 μm diameter polystyrene particles. The device exhibited a 85% separation efficiency. The approach was applied to separating SH-SY5Y neuroblastoma cells and C6 glioma cells with 80% efficiency and high relative viability (>90%). The simple planar structure and high sample throughput (> 1 million cells/min) offered by this passive microfluidic approach makes it attractive for many LOC devices for biomedical and environmental applications.

ACKNOWLEDGEMENTS

I would like to thank my advisor, Dr. Ian Papautsky, for his guidance during this work. His patience and constant encouragement have made working under him a very memorable and thoroughly enjoyable experience, and I feel deeply gratified to have been his student. I would also like to thank Dr. Jason Heikenfeld and Dr. Fred R. Beyette Jr. for being a part of my committee and for their valuable time and effort.

I would also like to extend my sincere regards to the entire Bio Micro Systems Lab for their continuous support and friendship. I would like to specially thank Ali Asgar Bhagat, for his mentoring and help with fabrication and characterization. It has been a great pleasure working with him. A special thanks are due to the staff at Micro/Nano Fabrication Engineering Research Center for their help with the cleanroom processing.

Finally and most importantly, I would like to thank my parents, Sathyakumar K.R. and Rajalakshmi V.R., for their support and encouragement, for always being there for me, for believing and supporting my decisions. I wish to dedicate this work to them.

TABLE OF CONTENTS

LIST OF FIGURES

Figure Page

LIST OF TABLES

CHAPTER 1

INTRODUCTION

Recent advancements in microfabrication and microfluidic technologies have resulted in emergence of numerous lab-on-a-chip (LOC) devices for biological and environmental applications. The subject has been reviewed extensively in recent literature [1-5]. These miniature LOCs are capable of performing analytical processes generally performed in large stationary chemical/biological laboratories. The advantages of using LOCs are that they require small sample volume, provide high throughput, allow automation of sample preparation and analysis, provide better accuracy, and can be lowcost and disposable [6-8]. Over the last decade, these microdevices have been developed for a number of applications, including PCR amplification [9-11], cell manipulation and separation [12, 13], DNA sequencing [14], and electrophoretic analysis [15-17]. LOC devices are typically composed of a network of microchannels, micro-pumps, micro-reservoirs, and other application-specific modules which are integrated together to perform complex sample analysis. Among these, the separation modules are indispensable in LOC devices developed for biomedical and environmental applications, and are generally used prior to sample analysis as a part of sample preparation. In most LOCs developed for biomedical applications, microparticle separator modules are employed for separating/isolating a particular cell type [18]. For example, efficient separation of human T-lymphocytes from whole blood is a critical step in the diagnosis and treatment of HIV disease. In another example, non-invasive prenatal diagnosis of fetal infections and birth defects can be

achieved by separating foetal cells from the maternal blood cells [18]. Microparticle separators can also be employed to isolate and thus concentrate testicular stem cells from testicular tissue for transplantation applications. Testicular transplantation procedure can be employed to restore fertility in patients suffering from testicular cancer [18]. In the case of LOC devices for environmental applications, the microparticle separator modules can be used to separate out harmful bacteria or metal nanoparticles in water quality analysis [18]. All these examples clearly demonstrate the need for high throughput continuous separation of microparticles.

In macroscale applications, porous membranes are traditionally employed for size-based separation of particles. This technique offers a simple and elegant way to quickly filter out particles of interest. However, on the microscale, the need for multiple stages to achieve multi-component separation requires complex fabrication steps, and issues arising from membrane clogging have limited the popularity of this approach. This has led to the development of a number of membrane-less separation techniques [19].

Microparticle separators

Based on the separation mechanism, microscale separators can be classified as active and passive devices. Active particle separators are those that utilize an external power source to manipulate the particle flow in microchannels. Conversely, passive particle separators make use of the hydrodynamic forces generated by fluid flow to differentially manipulate particles and thus achieve separation. Microparticle separators can be further classified into continuous and batch separators, based on their mode of operation. Separators working in batch mode, deal with a finite injected volume of particle solution at given point of time while in the case of continuous mode separators the sample fluid is continuously fed into the system. Continuous mode separators are more beneficial for LOC systems as they have minimum sample residence time

and can be easily integrated with other LOC modules. On the contrary, batch mode separators offer high accuracy and better separation efficiency [18, 19].

Active microparticle separators

The most commonly used active microparticle separation techniques include electrophoresis [20], dielectrophoresis (DEP) [21], magnetic separation [22-24], and optical fractionation [25, 26]. A detailed review on various other active microparticle separators can be found in recent literature [18, 19].

In electrophoretic separation, microparticles are separated by employing an uniform electric field. Particles of varying size and charge have different electrophoretic mobilities and hence migrate at different velocities towards appropriate electrodes when subjected to an external electric field. For instance, Xu *et al*. [20] employed a porous agarose gel in conjunction with an uniform electric field to successfully separate 5 nm, 10 nm, and 15 nm diameter spherical gold nanoclusters. Although this technique works well on the microscale, the requirement of having a charged particle restricts its relevance to a limited number of applications.

In dielectrophoresis, a non-uniform electric field is used to polarize and separate particles based on their dielectric properties. Since particle separation is dependent on the dielectric property of the particle, this technique can be employed to separate out both neutral and charged particles. For example, Yang *et al*. [21] demonstrated that by coupling the dielectrophoretic particle separation technique with cell specific antibody recognition, target bacterial cells can be efficiently separated from a composite cell mixture. In order to achieve this, they employed a non-uniform electric field to concentrate cells on a set of inter-digitated electrodes coated with target cell specific antibodies. Among the concentrated cells, the bacterial cells of interest bound

themselves to the antibodies on the surface of the electrode. Thus, when the electric field is deactivated the unbound cells got washed away by the flow while the cells of interest remained bound to the surface of the electrode. Although several dielectrophoresis based separation techniques, including the one mentioned above, have achieved close to 100% separation efficiencies, they all suffer from a critical disadvantage of being capable of only separating polarizable particles. Additionally, the high electric field and sample heating effects associated with DEP based techniques has limited its popularity in biological applications.

Magnetic microparticle separation is a simple and straightforward technique in which an external magnet is used to separate magnetic and non-magnetic particles. On the macroscale, magnetic microparticles coated with a layer of cell specific antibodies can be used to capture cells of interest with the help of an external magnet. This technique is commonly known as Magnetic Activated Cell Sorting (MACS). Deng *et al*. [23] successfully miniaturized this technique and were able to demonstrate near to complete separation of 4.5 μm diameter magnetic beads and 6 μm non-magnetic beads. However their technique operated in batch mode and thus suffered from a critical disadvantage of being a low throughput technique.

Pamme *et al*. [22] demonstrated a technique to continuously separate magnetic and non-magnetic particles on a microfluidic chip. In this example they used a non-homogenous magnetic field to differentially deflect magnetic particles having different magnetic susceptibilities. Thus, magnetic particles moving along the microchannel wall at the inlet are deflected to different positions by the magnetic field. The segregated particle streams are then collected using multiple outlets. The non-magnetic particles are not influenced by the magnetic field and thus continue to flow along the microchannel wall. Pamme *et al*. successfully employed this technique to separate out 2 μm, 4.5 μm diameter magnetic particles and 6 μm

diameter non-magnetic particles. Recently, Ingber *et al*. [24] developed a magnetic-microfluidic device to filter pathogens from diluted blood. In this approach, pathogens in the blood solution were tagged with magnetic beads and an external electro-magnet was employed to extract the magnetized pathogens thus, enabling continuous filtration of the blood solution. Although magnetic microparticle separation techniques are highly efficient and more importantly biocompatible, they suffer from reliance on magnetic particles.

Active particle separators are typically characterized by a very high separation efficiency and resolution. However, the need for an external force field necessitates complex fabrication processes and also results in integration issues. Moreover, since most techniques require a long particle residence time, active separators are often operated in batch mode thereby reducing their throughput. Finally, in the case of electrical separators, the high electric field can sometimes damage biological matter such as cells and fluids, thus making them incompatible with most biomedical applications. Due to these limitations, passive particle separators are more commonly employed in LOC devices.

Passive microparticle separators

Passive microparticle separators rely on the hydrodynamic force generated by fluid flow to separate particles based on their size. In these devices, channel geometry is used to control the hydrodynamic forces acting on the particles. The previously reported passive separation techniques include diffusion-based fractionation (H-Filter) [27, 28], pinched flow fractionation (PFF) [29], deterministic lateral displacement (DLD) [30-32], hydrodynamic chromatography (HDC) [33, 34], and inertial migration [35, 36].

H-filter is a microfluidic device that works on the principle of diffusion-based fractionation [27]. In this device the non-mixing, laminar nature of microfluidic flows and

difference in microparticle diffusivity is exploited to achieve size-based separation. The smaller particles have a larger diffusion coefficient and hence diffuse faster from the carrier fluid (particle laden solution) into the diluting fluid (particle free solution). On the other hand, the larger particles have a lower diffusion coefficient and hence remain in the carrier fluid. For instance, Jandik *et al*. [28] used the H-filter to separate and extract the antibiotic cephradine from blood. The H-filter offers a simple, passive, and membrane-less way to efficiently separate particles based on their size. However, the small diffusion coefficient of most large particles such a cells necessitates extremely long channel length to achieve any separation; making this approach impractical for cell separation applications.

In PFF, fluid flows with and without particles are introduced into microchannels comprising of a pinched and broadened segment. In the pinched segment, particles are aligned along the channel sidewall by controlling the flow rate of the fluid flow without particles [29]. As the particles travel from the pinched segment to the broadened microchannel segment, smaller particles experience a force directed towards the channel sidewalls while the larger particles experience a force towards the channel center. Due to the laminar nature of fluid flow in the microchannel, the difference in particle position in the pinched segment is amplified significantly in the broadened segment thus resulting in separate particle streams. For example, Yamada *et al*. [29] demonstrated this technique by efficiently (> 90%) separating 15 μm and 30 μm diameter polystyrene particles. Although PFF offers a simple way to separate particle mixtures, the need to have a narrow region introduces fabrication issues and also increases the pressure drop of system. Additionally, since the separation capability of this device is dependent on the dimensions of the narrow segment, this technique cannot be employed to separate microparticles over a wide range of particle sizes.

Deterministic lateral displacement relies on a carefully fabricated array of micro-pillars to achieve microparticle separation [30]. The micro-pillars are suitably placed in the microchannel such that particles larger than the critical diameter $d_c = 20\% \times 2w$ (w is the separation between two pillars) follow a deterministic path leading to the formation of multiple particle streams based on size. By stacking up micro-pillar arrays with different inter pillar distances, a wide range of particles can be continuously separated using this technique. Huang *et al*. [30] successfully demonstrated complete separation of 0.8 μm, 0.9 μm, and 1 μm diameter microspheres using this technique. DLD offers an elegant way to continuously separate microparticles over wide range of particle sizes. However, the presence of obstructions may lead to issues related to channel clogging and particle-particle interactions. Additionally, the reported throughputs are insufficient for cell sorting and flow cytometry applications.

In HDC, the parabolic nature of the velocity profile in a pressure driven flow is exploited to separate particles based on their size [33]. In this technique, a high aspect ratio microchannel with one of the dimensions comparable to that of the particle size is employed to achieve separation. Larger particles flowing through a narrow microchannel cannot fully access the low velocity regions near the channel wall and hence are relatively more present at the center of the microchannel. As a result the larger particles move faster than the smaller particles and can thus be separated. Chmela *et al*. [33] employed a 1 μm deep channel to efficiently separate 26 nm, 44 nm, and 110 nm diameter particles. Similar to DLD, the HDC technique suffers from being a low-throughput microparticle separation technique.

Inertial microfluidics offers a simple way to filter out a wide range of particles using a simple straight microchannel [35-37]. In these microparticle separators neutrally buoyant particles, under the influence of fluid shear induced inertial forces, migrate to stable equilibrium

positions along the channel periphery. By modulating the aspect ratio of the microchannels the microparticles can be made to align along the side wall of the microchannels and then filtered out by using appropriate outlets. Bhagat *et al.* [35] successfully demonstrated filtration of 1.9 μm diameter particles using this technique. Furthermore, Di Carlo *et al.* [36, 37] showed that using a curvilinear channel, Dean vortices can reduce the number of equilibrium positions to one. This single particle stream can later be extracted by employing bifurcated outlets. Using this approach rapid microparticle filtration has been demonstrated recently. Chapter 2 contains a more detailed discussion of the various types of curvilinear separators.

Overall, passive microparticle separation techniques have a higher throughput and are much easier to fabricate compared to their active counterparts. Additionally, passive microparticle separators operate in continuous mode thus making it easy to integrate them with other LOC modules. The disadvantages of passive microparticle separators, however, include the lower separation efficiency and the ability to separate microparticles based on size only.

Motivation and scope

Our laboratory recently introduced a technique to completely separate two neutrally buoyant particles based on their size using inertial lift and Dean drag forces in spiral microchannels [38]. The developed spiral design took advantage of the inertial lift and viscous drag forces acting on particles of various sizes to achieve differential migration, and hence separation of microparticles. The dominant inertial forces and the Dean drag forces due to the spiral microchannel geometry caused the larger 7.32 μm diameter particles to occupy a single equilibrium position near the inner microchannel wall. The smaller 1.9 μm diameter particles migrated to the outer half of the channel, primarily under the influence of Dean drag forces

resulting in the formation of two distinct particle streams which are collected in two separate outputs.

The spiral separator described above can be employed to separate only two particles of different size. The goal of this work was to further investigate the principle of Dean coupled inertial migration and to use it to demonstrate a complete multi-particle separation. Additionally, the low throughput of the previously developed device provided the motivation to develop a technique to rapidly and simultaneously separate multiple particles. To achieve this, a 5-loop Archimedean spiral microchannel was designed and fabricated using standard soft lithography process. A bifurcated outlet system was designed to ensure efficient collection of the separated particle streams. The device was used to demonstrate separation of 10 μm, 15 μm, and 20 μm diameter particles. A sample application in cell sorting was demonstrated by separating SH-SY5Y neuroblastoma cells and C6 glioma cells.

Chapter summaries

Following the introduction, Chapter 2 contains a discussion of the physical principles of microparticle separation using curvilinear channels. Chapter 3 details the methodology involved in fabricating and characterizing the spiral microfluidic device. The experimental results are presented and discussed in Chapter 4. Chapter 5 briefly summarizes this work and draws conclusions.

CHAPTER 2

CURVILINEAR MICROPARTICLE SEPARATORS

In curvilinear microparticle separators, the centrifugal acceleration introduced due to the curvilinear nature of the channel geometry is used to achieve size-based separation of microparticles [37, 38]. The passive, membrane-less, continuous flow nature of this approach makes it ideal for most LOC applications. This chapter discusses the basic physics behind this technique. Additionally, recent demonstrations of microparticle separations using curvilinear channel geometry have also been discussed.

Dean flows

The centrifugal acceleration component acting on a fluid flowing through a curvilinear microchannel results in the formation of two counter rotating vortices on the top and bottom halves of the microchannel cross-section as shown in Figure 1. Thus, in a curvilinear channel the fluid flow can be visualized to form a helical flow pattern because the fluid also has a velocity component that is perpendicular to the normal flow direction. These secondary flow vortices are also known as Dean vortices and their magnitude can be quantified by a dimensionless number known as the Dean number (*De*) which is given by:

$$De = \frac{\rho \overline{U} D_h}{\mu} \sqrt{\frac{D_h}{2R}} = \mathrm{Re} \sqrt{\frac{D_h}{2R}} \qquad (1)$$

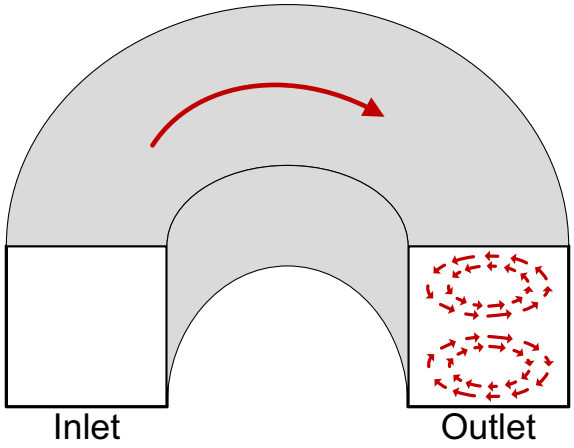

Figure 1. Schematic illustrating the formation of two counter rotating Dean vortices in the top and bottom half of a curvilinear microchannel.

where ρ is the density of fluid medium, $\overline{U}$ is the average fluid velocity, μ is the fluid viscosity, R is the radius of curvature of the path of the curvilinear channel, and Re is the flow Reynolds number [39-42]. As indicated by the above expression, the magnitude of secondary flows is directly proportional to the flow velocity and channel cross-sectional dimension and inversely proportional to the radius of curvature of the microchannel. Hence, a straight channel with an infinite radius of curvature has no secondary flows. Conversely, the magnitude of the Dean vortices increases as the microchannel radius of curvature reduces. For a given Dean number, the expression for the average Dean velocity ($\overline{U}_{Dean}$) was given by Ookawara *et al.* to be

$$\overline{U}_{Dean} = 1.8 \times 10^{-4} De^{1.63} \tag{2}$$

In the case of a particle laden fluid flowing through a curvilinear microchannel, the Dean vortices exert a drag force known as the Dean drag force (F_D) on the suspended particles. Assuming Stokes drag, the expression for the magnitude of the Dean drag force exerted on a particle is given by

$$F_D = 3\pi\mu\overline{U}_{Dean}a_p = 5.4 \times 10^{-4}\pi\mu De^{1.63}a_p \tag{3}$$

where a_p is the microparticle diameter [38]. As seen in the expression above, the magnitude of drag force experienced by the particles is dependent on the size of the particle.

Inertial microfluidics

In a plane Poiseuille flow, suspended particles with an $a_p/D_h \geq 0.07$ experience a shear gradient induced inertial lift force due to the parabolic nature of the velocity profile. This shear induced inertial lift force (F_{SL}) is responsible for driving the suspended microparticles away from the microchannel center and towards the channel walls. As the particle moves closer to the channel wall, the rotational wake around the particles is disturbed due to the presence of the wall. This results in particles experiencing a lift force known as the wall induced lift force (F_{WL}) that is directed away from the wall as shown in Figure 2. These oppositely directed forces cancel out and thus the particles equilibrate at a distance of ~$0.2D_h$ from the channel center. At this point particles are only subject to the viscous drag force (F_{VD}) due to the fluid flow [36, 43-44].

Segre and Silberberg [45, 46] were the first to report this effect. They showed that in a sufficiently long channel, a uniformly distributed suspension of neutrally buoyant particles at the inlet form a narrow band at $0.6R$ (Figure 3(a)) where R is the radius of the circular channel. However, in the case of channels with rectangular and square cross-sections the particles tend to equilibrate at discrete equilibrium positions instead of forming a continuous ring as shown in Figure 3(b) [47].

The shear induced inertial lift force acting on the particle is dominant at the channel center and the wall induced lift force dominates when the particle is close to the channel walls. Hence the net lift force $(F_L = F_{SL} + F_{WL})$ acting on the particle is a function of the position of the particle across the channel cross-section and is given by:

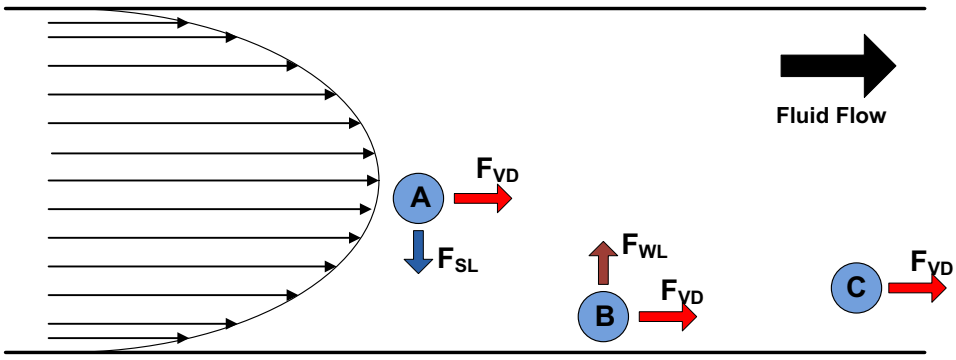

Figure 2. Schematic illustrating the lift forces acting on a particle in a parabolic flow. Particle at the center of the microchannel (*A*) experiences a dominant shear-induced lift force (F_{SL}). Particles closer to the microchannel wall (*B*) experience a dominant wall induced lift force (F_{WL}). Particles at the equilibrium position (*C*) are only subject to the viscous drag force (F_{VD}) due to the fluid flow.

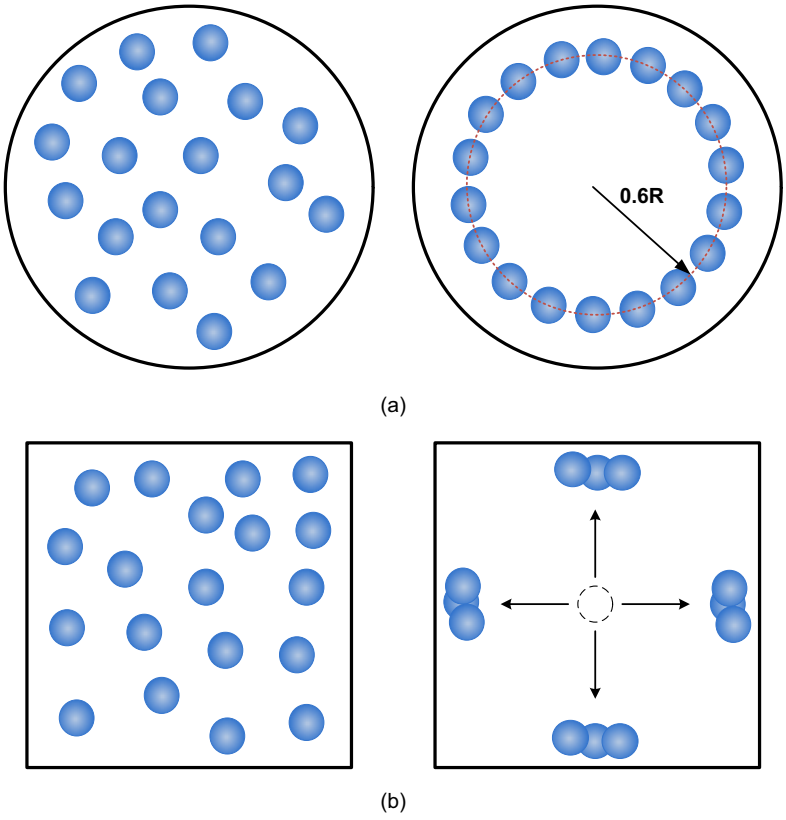

Figure 3. Inertial migration in circular and square channels. (a) Particles uniformly distributed at a circular channel inlet equilibrate and form a narrow band at a distance of 0.6*R* from the channel center. (b) In square channels, particles form a broken band and equilibrate at each of the channel wall centers.

$$F_L = \rho G^2 C_L a_p^{\ 4} \tag{4}$$

where G is the shear rate of the fluid given by $G = U_{max}/D_h$, U_{max} is the maximum fluid velocity and C_L is the lift coefficient. The magnitude of lift coefficient and hence the lift force rises from zero at the channel center to a maximum value before falling back to zero again at a distance of ~$0.2D_h$ away from the channel wall, equilibrating the particles [44]. Beyond this point, the lift coefficient changes sign indicating a dominance of wall-induced lift force.

The above expression clearly shows dependence of the lift force on the fluid shear rate. Hence, by modulating the fluid shear rate the particles can be forced to preferentially equilibrate at certain equilibrium positions across the channel cross-section. Bhagat *et al.* [35] recently demonstrated that in a low aspect ratio (ratio of channel height H to channel width, W) microchannel, the high shear rate along the channel height results in a preferential equilibration of particles along the top and bottom channel walls as shown in Figure 4.

Finally, the lift coefficient (C_L) is dependent on the flow Reynolds number and the position of the particle. Since the lift coefficient is independent of the particle size, all particles of different sizes equilibrate at the same position ($C_L = 0$) for a given Re. Therefore, it is not possible to separate particles solely based on the inertial forces [37]. However, by introducing a

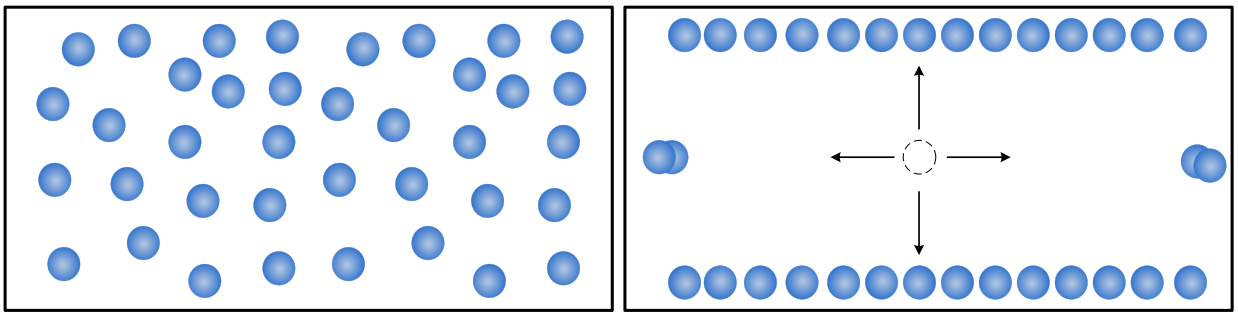

Figure 4. Shear induced preferential migration in low aspect ratio channels.

competing force with a magnitude of the same order as that of the inertial lift force, particles can be made to equilibrate at different positions across the microchannel cross-section. By employing a curvilinear channel, the Dean drag force can be used in conjunction with the inertial lift force to differentially equilibrate microparticles based on their size. This is the basic principle of operation behind most curvilinear microparticle separators. The subsequent section contains a brief discussion of some of the recently reported separators.

Curvilinear microparticle separators

In a curvilinear microchannel, the trajectory of a particle with an $a_p/D_h \geq 0.07$ is influenced by both the inertial lift force and the Dean drag force. The particle experiences either a dominant inertial force or a dominant Dean drag force depending on its position across the microchannel cross-section. Figure 5 illustrates a cross-sectional view of a curvilinear microchannel iindicating the various forces acting on the particles at different positions across the channel cross-section.

Particles at the top and bottom channel walls experience a dominant Dean drag force and are entrained in one of the two Dean vortices. In the case of particles near the outer wall of the microchannel the inertial lift force supplements the Dean drag force and hence the particle stays entrained in the Dean vortex. Towards the inner microchannel wall, the inertial lift force opposes the Dean drag force and hence the particle equilibrates at a position where the two forces balance each other. The Dean drag force is instrumental in reducing the four equilibrium positions seen in a straight microchannel Figure 3(b) to a single equilibrium position (inner microchannel wall). Particles uniformly dispersed at the channel inlet, equilibrate at the center of the inner channel wall, thus forming a single stream of particles. Due to the laminar

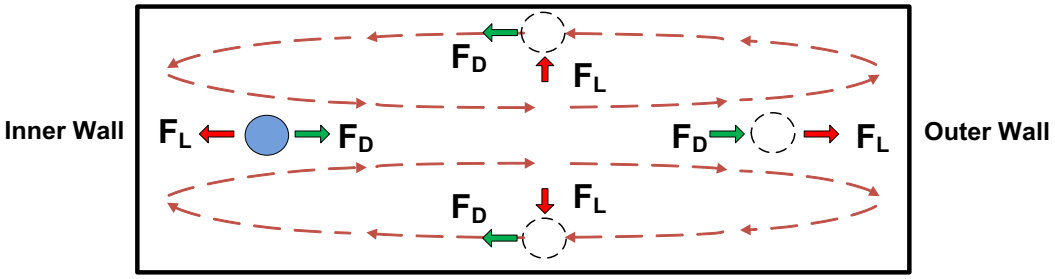

Figure 5. Schematic illustrating the direction of the net inertial lift (F_L) and Dean drag forces (F_D) acting on particles at various positions across the microchannel cross-section. The hollow circles indicate the unstable equilibrium positions and the solid circle represents the stable equilibrium position.

nature of microchannel flows, suitable outlets can be design to extract the single particle stream. On the other hand particles with an $a_p/D_h \leq 0.07$ experience a dominant Dean drag force and thus stay entrained in one of the two Dean vortices [38].

Finally, it must be noted that the Dean drag force is responsible for transporting the particles to their final equilibrium position. By operating at higher Dean number ($0 < De < 20$), the particles can be made to quickly reach their equilibrium position thus achieving separation/filtration in shorter channel lengths. However, at very high Dean numbers ($De > 20$) the Dean drag force dominates the inertial lift force at all positions across the channel cross section and all the particles get entrained in the two Dean vortices. Hence, to achieve particle equilibration, the device must be operated at $De < 20$.

Gregoratto *et al.* [48] used a spiral microchannel to demonstrate continuous filtration of large volumes of dilute particle suspensions. In order to minimize the dispersive effect of Dean vortices, they fabricated a high aspect ratio spiral microchannel (100 µm × 1250 µm) with one inlet and two outlets in silicon using the standard DRIE process. They then tested the device with 1 µm, 8 µm, and 10 µm diameter particles polystyrene particles. They found a 3.5 and a 2 times increase in the concentrations of 10 µm and 8 µm diameter particles in one of the channel

outlets at an input velocity of 0.27 m/s (flow rate of 2 mL/min). As expected, the concentration enhancement in the case of 1 μm diameter particles was negligible. They also reported higher particle concentration enhancements with longer spiral channel lengths (~75 cm). One of the main advantages of using a spiral channel is the fact that longer channel lengths can be achieved in lower area, thus making it ideal for LOC applications.

Seo *et al.* [49, 50] also employed a spiral microchannel to demonstrate particle filtration. In order to achieve long channel lengths in smaller area, they intertwined two spiral channels by adding a "S" shape microchannel unit at the center. By fabricating a spiral with a very long channel length, they were able to achieve a 200 fold increase in concentration of 10 μm diameter polystyrene particles at a flow velocity of 92 mm/sec. They also achieved a 9.3 and 1.4 times concentration enhancement with 6 μm and 3 μm diameter polystyrene particles.

Di Carlo *et al.* [36] demonstrated particle focusing in both symmetric and asymmetric serpentine microchannels. In the case of symmetric microchannels, they observed that the four equilibrium positions in the case of a straight rectangular channel reduce to two (one at the inner and outer channel walls). This is primarily because of the fact that in the case of a symmetric serpentine microchannel, the Dean vortices reverse directions at each bend. By employing an asymmetric serpentine microchannel, the magnitude of Dean vortices in the narrower bend dominates and the particles tend to focus into one single stream. Di Carlo *et al.* also fabricated a channel with multiple outlets to partially separate out 10 μm and 2 μm diameter particles. In an asymmetric serpentine microchannel ($\overline{H}$ = 50 μm), the 10 μm diameter particles focus into a single stream, while the 2 μm diameter particle remain dispersed across the width of the microchannel. Hence, by using a channel with multiple outlets, a pure solution of 2 μm diameter particles and a concentrated solution of 10 μm diameter particles can be obtained as shown in

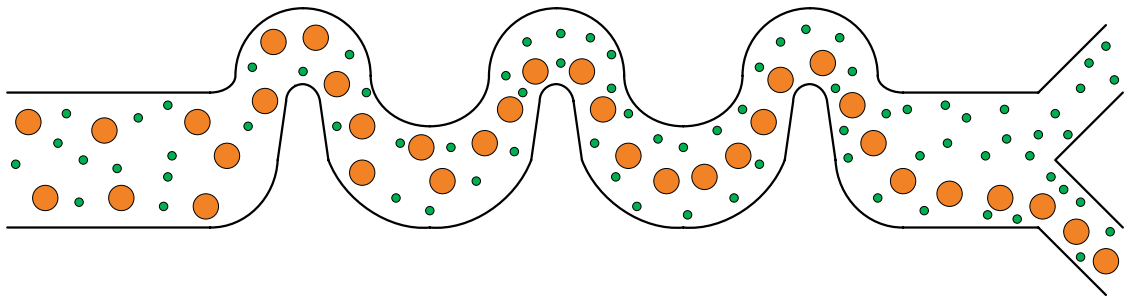

Figure 6. Schematic illustrating the filtering of 10 μm particles from a mixture of 10 μm and 2 μm diameter particles using serpentine microchannels [36].

Figure 6. They also demonstrated that cells (RBC) behave in a manner similar to that of neutrally buoyant particles.

Recently, Bhagat *et al.* [38] showed that by dispersing particles across half the channel width (instead of across the channel width) as shown in Figure 7, complete separation of two different particle sizes can be accomplished. They used a two inlet, two outlet spiral microchannel with a cross-sectional dimension of 100 μm × 50 μm to separate out 7.32 μm ($a_p/D_h = 0.11$) and 1.9 μm ($a_p/D_h = 0.02$) diameter particles. Particle laden solution was pumped in through one of the inlets while pure DI water was pumped in through the other. The laminar nature of microchannel flows resulted in two parallel streams as shown in Figure 7. The 1.9 μm diameter particles experience a dominant Dean drag force and hence are fully entrained in one of the two Dean vortices. The 7.32 μm diameter particles experience a dominant inertial lift force and thus equilibrate at the inner microchannel wall. By choosing an appropriate channel length and fluid flow velocity, the Dean velocity can be adjusted such that the band of 1.9 μm diameter particles shifts from the inner wall at the inlet to the outer wall at the channel outlet. Thus, with a bifurcated outlet system the 7.32 μm diameter particles can be collected at the inner outlet and the 1.9 μm diameter particles can be collected at the outer outlet, as shown in Figure 7.

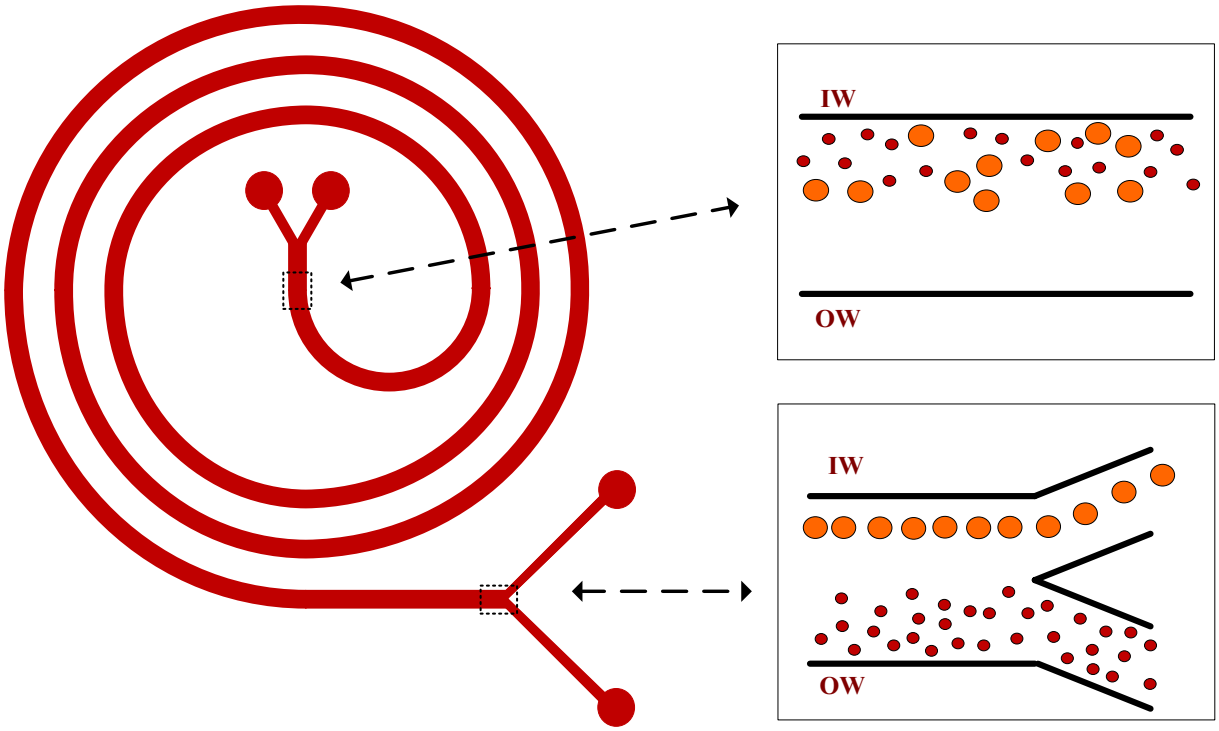

Figure 7. Schematic illustrating the complete separation of 7.32 μm and 1.9 μm diameter particles using spiral microchannels [38].

Summary

Particles flowing through a spiral microchannel experience a combination of inertial lift and Dean drag forces. Under the influence of these two forces, particles dispersed uniformly at the channel inlet equilibrate at the inner microchannel wall at the outlet. Thus, a single ordered stream is formed. Since the inertial and Dean drag forces acting on the particles increase with flow rates, inertial microfluidics can be used for microparticle separations. The next chapter will discuss how these principles of inertial microfluidics can be used to passively separate particles at high throughput.

CHAPTER 3

EXPERIMENTAL METHODS

This chapter discusses experimental methods used to develop the spiral multi-particle separator. The first section details design parameters that influence particle focusing and separation efficiency of the spiral microparticle separator. The subsequent section briefly describes the various steps involved in fabricating the spiral microchannel using the standard soft lithography process. The final third section contains a detailed discussion of the device characterization techniques methodology.

Spiral microchannel design

To separate microparticles using a spiral microchannel, particles need to be focused into distinct streams and then collected using a suitable outlet system. The two important parameters affecting separation efficiency are the particle size to channel height ratio (a_p/H) and the spiral microchannel length. Both parameters are discussed in detail in this section.

Particle size to channel height ratio

The particle size to channel height ratio (a_p/H) defines the range of particle sizes that can be separated in a spiral channel of given cross-sectional dimensions. Bhagat *et al*. [35] showed that particle equilibration in microchannels with a rectangular cross-section depends on the shortest channel dimension (microchannel height, H) rather than hydraulic diameter D_h, due to

the dependence of shear rate on the channel dimension. They showed that in the case of low aspect ratio rectangular microchannels, the criterion for particle focusing is $a_p/H \geq 0.07$. Thus, for a given microchannel height the lower particle size limit that will focus into a single stream is given by $0.07H$. From a practical standpoint, issues related to channel clogging and particle-particle interactions limit the largest particle diameter that can be run through a microchannel of height H to around $0.3H$. Therefore, in a spiral microchannel with a cross-sectional dimension of 500 μm × 120 μm, (H = 120 μm), the particle sizes that can be separated range from 8 μm ($0.07H$) to 40 μm ($0.3H$) in diameter.

As mentioned in Chapter 2, particles flowing in a spiral microchannel with rectangular cross-section experience a combination of lift and Dean drag forces. The magnitude and direction of these forces depends on the particle size and position across the microchannel cross section. In the case of particles with an $a_p/H \geq 0.07$, the lift forces dominate and are responsible for the particles equilibrating at the inner wall of the microchannel. However, the position at which at the particles equilibrate is dependent on the ratio of the inertial lift to Dean drag force acting on the particle. Since the ratio of the two forces acting on the particle scales with the third power of the particle size ($F_L/F_D \alpha (a_p/H)^3$), a wide range of closely spaced particles (< 1 μm) can be made to equilibrate at different positions across the microchannel cross-section and thus separated by using a wider, low aspect ratio spiral microchannel (Figure 8). In this work, a 500 μm × 130 μm spiral channel was employed to separate 10 μm (a_p/H = 0.076), 15 μm (a_p/H = 0.11), and 20 μm (a_p/H = 0.15) diameter particles.

Spiral microchannel length

In a spiral microchannel, the inertial lift forces are responsible for particle migration and equilibrating along the channel periphery as explained in Chapter 2. The particles at the outer,

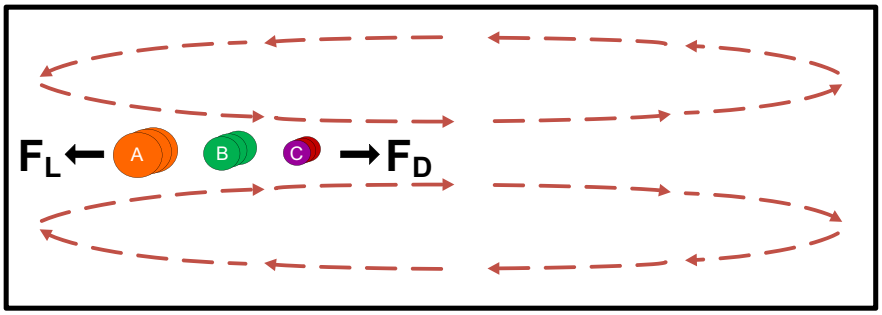

$$\left[\frac{F_L}{F_D}\right]_A > \left[\frac{F_L}{F_D}\right]_B > \left[\frac{F_L}{F_D}\right]_C$$

Figure 8. Microchannel cross-section illustrating effects of F_L and F_D on particles. The ratio of forces (F_L/F_D) is the determining factor in where a particle of given size (diameter) equilibrates.

top and bottom channel walls are influenced by the Dean drag force and thus migrate towards the inner microchannel wall. Thus, in order to form a single ordered stream of particles, the spiral microchannel must be sufficiently long enough to ensure that all the randomly dispersed particles at the channel inlet migrate and equilibrate at the inner wall before they reach the outlet region. The minimum channel length required to achieve complete focusing is given by

$$L_T = \left(\frac{U_a}{\overline{U}_{Dean}}\right) \times L_M \tag{5}$$

where L_T is the minimum channel length required. L_M is the Dean migration length of the microparticle and is approximately equal to twice width of the microchannel.

Since the magnitude of the Dean drag force is dependent on the curvature of the curvilinear channel, the developed spiral microdevice was designed with a radius of curvature of 1 cm so as to ensure that the Dean drag force on each of the particles is comparable to that of the inertial lift force acting on the particle. The length of the spiral microchannel was fixed at 40 cm in order to ensure that three particles of interest focus even at lower flow rates and thus the number of loops in the developed Archimedean spiral design was fixed at five.

Finally, to achieve a good separation between individual particles, the segregated particle streams need to be efficiently collected into separate outlets. The overall performance of the spiral microparticle separator depends on the collection efficiency of the outlet design. In this work the laminar nature of microfluidic flows was exploited by opening up the 500 µm wide channel into a 1 mm wide section in order to enhance the separation between the individual particle streams.

The schematic of the developed device is shown in Figure 9. The dependence of ratio of the lift force to the Dean drag force on particle size and the shear rate modulation in low aspect ratio microchannels have been exploited to demonstrate complete separation of 10 µm, 15 µm, and 20 µm diameter

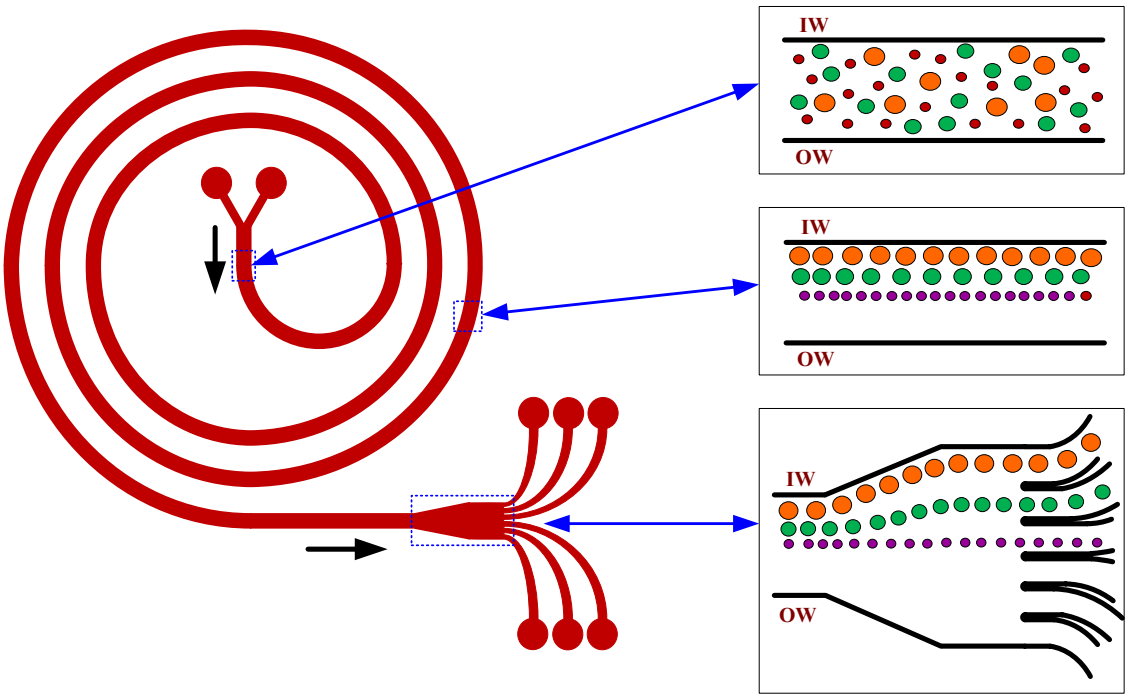

Figure 9. Schematic of the spiral microparticle separator. The randomly dispersed particles equilibrate at different equilibrium positions along the inner wall (IW) of the spiral microchannel under the influence of F_L and F_D. Separation between individual particle streams is enhanced by opening the spiral channel into a wider straight channel before extracting the individual streams using the eight equally spaced outlets.

particles. The dominant inertial lift forces will align the randomly distributed particles at the inlet near the inner microchannel wall as the flow progresses downstream. The significant Dean drag force will move these focused streams farther away from the channel wall depending on the particle size, with the largest particle being closest to the inner channel wall, resulting in evolution of three distinct particle streams that can be independently

Fabrication

The spiral microfluidic channels were fabricated using the standard two step soft lithography process. In the first step, master was fabricated by patterning SU-8 on a 6" silicon master using the UV-lithography process [51]. Then, polydimethyl-siloxane (PDMS) was cast on to the silicon master and allowed to cure. The cured PDMS was peeled off and bonded to glass to form the final device. Each of the above mentioned steps have been explained in details in the subsequent paragraphs. The device was fabricated using PDMS because of its various advantages such as low cost, ease of fabrication, good reproducibility and above all optical transparency.

Figure 10 shows a schematic of the various fabrication steps involved. Given the large dimension of the developed design, a 6" Silicon wafer was used to fabricate the master. In the first step, the single-side polished silicon wafer was cleaned with acetone, methanol and iso-propyl alcohol and finally DI water for 3 min each, in order to remove any organic impurities on the wafer. The silicon wafer was then dipped in Buffered Oxide Etchant (BOE – 3:3:1 of H_20: NH_4F: HF) for about 25 sec in order to remove any native oxide layer on the silicon wafer. This step was done to ensure proper adhesion between the silicon wafer and the SU-8 photoresist. Following the native oxide removal step, the silicon wafer was dried using N_2 and dehydrated on

a ceramic hot plate at 150 ˚C for 10 min and then cooled to room temperature before spin coating negative photoresist SU-8 2075 (MicroChem Corp., MA).

Spin coating of the photoresist onto the silicon substrate was carried out in two steps. In the first step, approximately 20 ml of negative photoresist was deposited onto the silicon substrate and the silicon wafer was ramped up to 500 rpm at the rate of 100 rpm/sec and held for 10 sec. This step was done to dispense the photoresist across the silicon substrate. In the second step, in order to obtain a photoresist thickness of 130 μm, the wafer ramped up from 500 rpm to 1100 rpm at the rate of 200 rpm/sec and held for 45 sec. Following spin coating, the wafer was kept on a leveled plate for about 10 min so as to allow the photoresist to relax.

Subsequently, the wafer was transferred on to a temperature controlled aluminum hot plate for the pre-bake step. During this step, the wafer was initially heated to 65 ˚C and held at

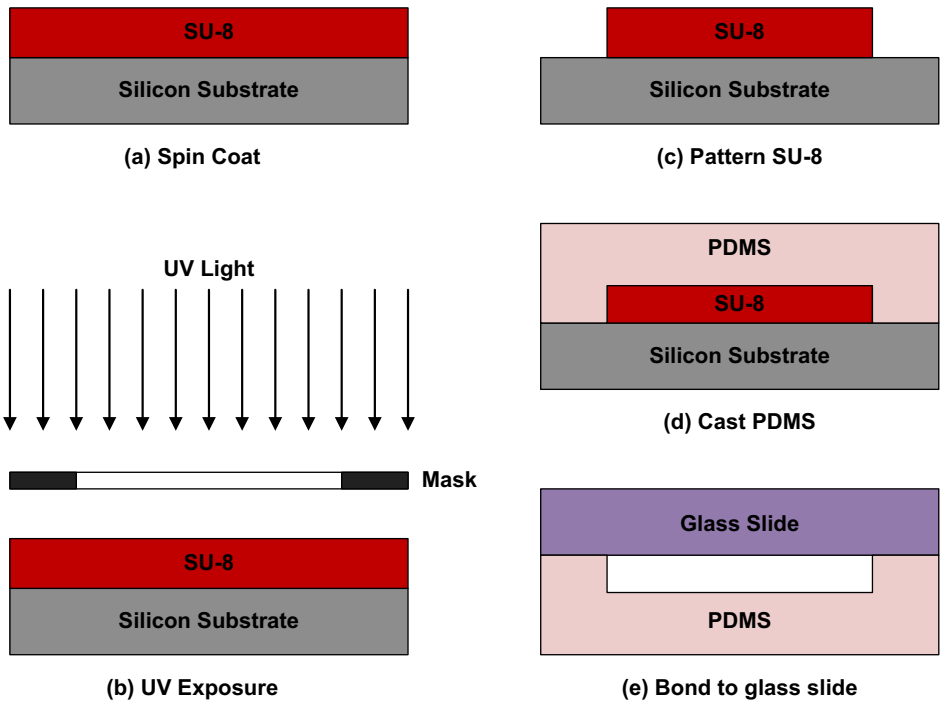

Figure 10. Schematic showing the various steps involved in fabricating a PDMS microfluidic device using a SU-8 silicon master.

that temperature for about 5 min. The temperature of the hot plate (with the wafer on it) was ramped up to 95 ˚C (at ~5 ˚C/min) and held at that temperature for about 25 min. This pre-exposure bake step was carried out to improve the adhesion between the photoresist and the silicon substrate. This procedure also aids in removing any residual solvent and stresses in the photoresist. After the pre-exposure bake, the wafer was allowed to cool down to room temperature before UV-exposure.

The deposited photoresist was patterned by exposing it to UV light. The resist was exposed at 300 mJ/cm^2 (5 mW/cm^2 for 60 sec) using an I-line (365 nm) high pass filter. A layer of glycerin was added between the mask and the silicon substrate so as to avoid any air gaps. Glycerin with a refractive index similar to that of glass and the photoresist was essential to reduce refraction of light and thus help in obtaining vertical aside-walls. Following UV-exposure, the wafer was once again left on a leveled plate for 10 min before carrying out the post exposure bake procedure. As in the pre-exposure bake step, here again the wafer was initially heated to 65 ˚C and held at that temperature for about 5 min. Following that, the temperature of the wafer was ramped up to 95 ˚C (at ~5 ˚C/min) and held at that temperature for about 10 min. Finally the wafer was allowed to cool back to room temperature before the developing step.

In order to remove the excess (un-exposed) photoresist, the wafer was dipped in a container filled with SU-8 developer. The wafer was continually agitated so as to ensure proper penetration of the developer liquid and thus proper formation of "U" shape grooves in the design. After the development process, the wafer was rinsed in DI water, dried with N_2 and descummed in O_2 plasma (20 sccm, 13.56 MHz) for 6 min at 300 W. Finally to ensure easy removal of PDMS cast a few drops of Sigmacote (Cat # SL-2, Sigma Aldrich) was pippetted onto the wafer and allowed to air dry for about 30 min.

The PDMS mixture was prepared by mixing ten parts of PDMS elastomer base with one part of the curing agent (10:1). The mixture was properly stirred, degassed and poured onto the silicon master. The PDMS was then cured on a hotplate at 80 ˚C for 2.5 hours. Following that, the cured PDMS was carefully cut, peeled off and the inlet and outlet holes were drilled in using a razor sharp 14 gauge needle. The PDMS device mold along with a 2"×3" glass slide were rinsed in 5:1 (v/v) ratio of H_2O and HCl and blown dry using N_2 blower. The PDMS mold was then finally bonded to the glass slide using corona wand treatment (BD-20AC, Electro-Technic Products).

Characterization

Fluorescently-labeled polystyrene particles from Bangs Laboratories were diluted in DI water before testing (volume fraction ~ 0.05%). During testing, two syringes filled with the diluted particle solution were driven at a varying flow rates using a syringe pump (KDS101, KD Scientific). Particle flow in the microchannel was observed using an inverted epi-fluorescence microscope (Olympus IX71) equipped with a 12-bit CCD camera (Retiga EXi, QImaging). The experimental setup comprising of a inverted epi-fluorescent microscope, syringe pump and spiral microfluidic device is shown in Figure 11.

To determine position of the focused particle stream across the microchannel cross-section, a 300 frame video of the particle flow was captured using the CCD camera. ImageJ® software was then used to split the video file into individual frames and generate a Z-stacked average composite image by overlaying each of the 300 images. The inset in Figure 12 contains a fluorescent image of the focused 15 μm diameter particle in a 500 μm wide section of the spiral microchannel. The corresponding grayscale line scan showing the normalized pixel intensity across the 500 μm wide channel is also shown in Figure 12.

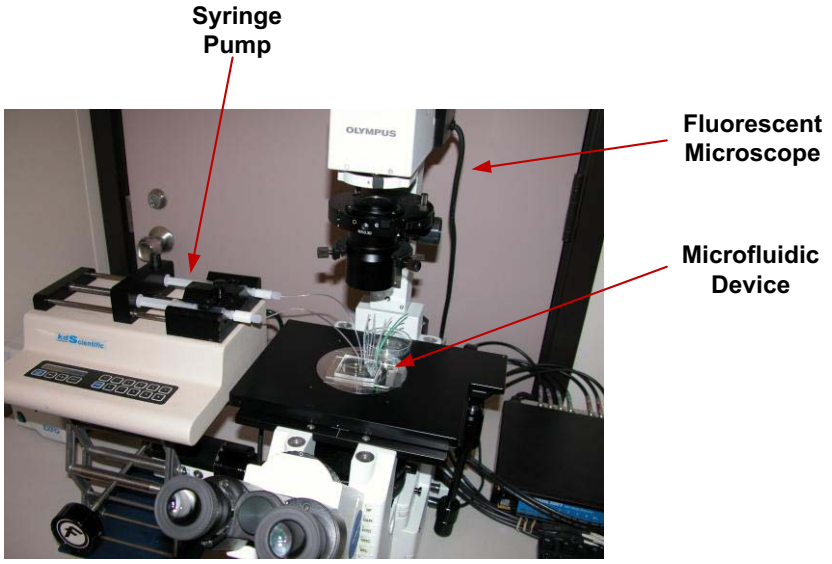

Figure 11. Photograph of the experimental setup showing the fluorescent microscope, syringe pump, microfluidic device.

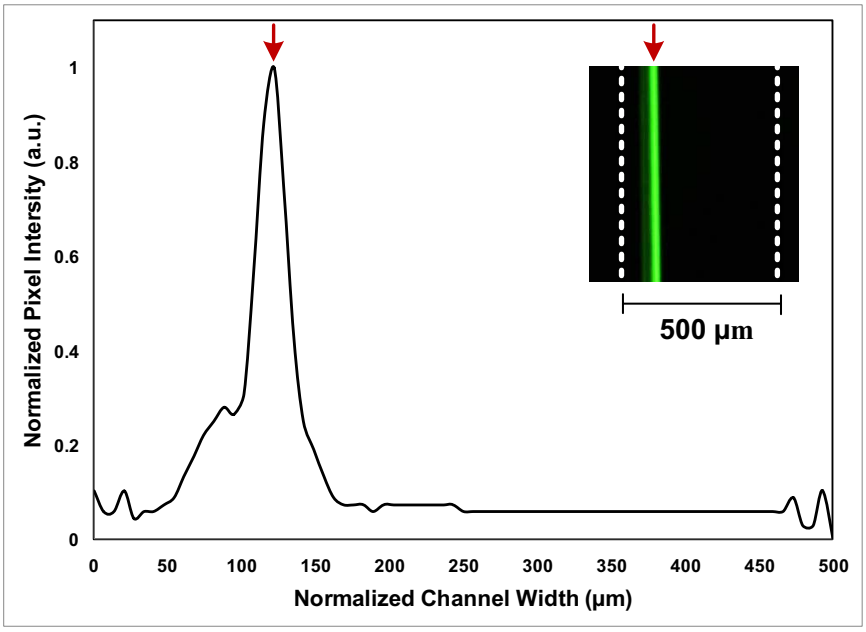

Figure 12. Cross-sectional line scans indicating the normalized pixel intensity of a focused 15 μm particle stream in the 500 μm wide section of the spiral microchannel.

The peak corresponds to the particle and the kinks on either ends of the graph correspond to the microchannel walls. In order to demonstrate separation a homogenous particle mixture solution, containing the particles mentioned in Table 1 was pumped through the inlet. The particle streams were viewed and captured separately using appropriate filter cubes. Finally the individual images were super-imposed to create a composite image to display the formation of three separate particle streams.

To quantify separation efficiency, outlet streams at each of the eight outlets were collected in separate vials and analyzed by flow cytometry. The LSR BD II flow cytometer was used to perform the analysis. Individual particles solutions were used as controls to draw the gates on a FSC vs SSC plot. The collected samples were then run to determine the particle count for each of three particles in all the eight outlets.

To demonstrate cell separations, SH-SY5Y neuroblastoma cells ~ 15 μm (σ = 5 μm) in diameter were cultured in Opti-MEM medium containing 10% fetal bovine serum supplemented with L-glutamine. The rat glioma cells, C6, ~ 8 μm (σ = 3 μm) in diameter were cultured in Ham's F-12 medium containing 15% horse serum and 5% fetal bovine serum supplemented with 0.25 μg/mL amphotericin B, 100 U/mL penicillin, and 100 μg/mL streptomycin. Both cultures were maintained at 37^{o}C in a humidified atmosphere containing 5% (v/v) CO_2. Cells were

Table 1. Summary of the particle sizes used in this work.

Particle size (μm)	Particle size distribution σ (μm)	Flurophore
10	0.54	DAPI
15	0.98	FITC
20	0.5	TRITC

cultured in sterile 25 cm^2 flasks (Corning). Cells were subcultivated (1:4) three times a week and media was replaced every 48 hours. Sub-confluent monolayers were dissociated with 0.01% trypsin and 5.3 mM EDTA solution, re-suspended in fresh basal media with 5% serum for further subculture. Cells were never allowed to reach 100% confluent. Prior to testing, the cells were mixed together and diluted in 1× phosphate buffered saline (PBS) solution (volume fraction 0.05%). The SH-SY5Y neuroblastoma cells were labeled with CellTracker™ Green (Invitrogen Corp., Carlsbad, CA) for better visualization and to confirm separation. The PDMS based devices were thoroughly flushed with PBS and antibiotics (1× PSN) before running the cell mixture and all experiments were conducted in a sterile environment.

CHAPTER 4

RESUTLS AND DISCUSSION

This chapter presents fabrication and experimental results of this work. The first section illustrates the spiral microchannels fabricated. In the second section, the results from both the individual particle experiments and the particle mixture experiments have been presented and analyzed. The final section describes the results obtained from running cells through the developed spiral microchannel device.

Devices

The final fabricated devices consisted of a five loop Archimedean spiral microchannels with two inlets and eight equally spaced outlets. Figure 13 shows the photograph of the fabricated spiral microchannel along with the scanning electron microscope picture of the outlet section. The spiral designs had an initial radius of curvature of 1 cm, with spacing between the successive spiral loops fixed at 500 μm and a total channel length of 40 cm. To study particle focusing in the designed spiral microchannels, the microchannel width was fixed at 500 μm with height varying from 90 μm – 140 μm. At the outlet, the 500 μm wide channel opened into a 1 mm wide segment to increase spacing between particle streams by taking advantage of the laminar nature of microchannel flows. Finally, the 1 mm wide section was split evenly into eight 100 μm wide outlets.

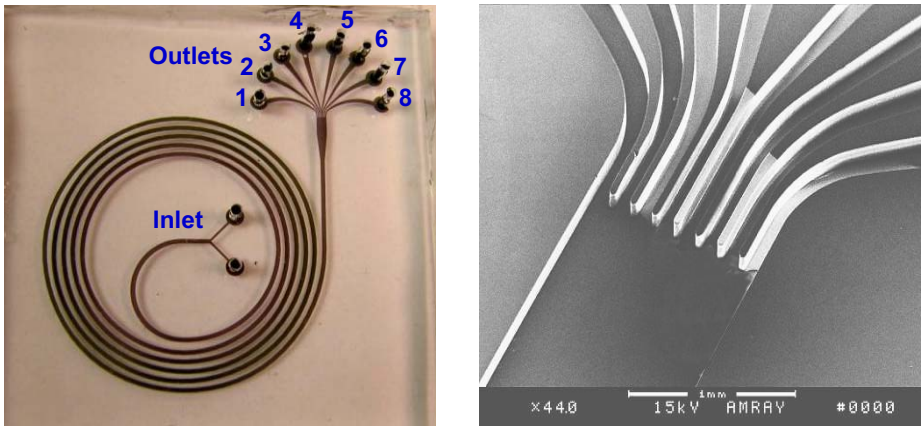

(a) (b)

Figure 13. (*a*) Photograph of the 5-loop spiral microchannel with two inlets and eight outlets fabricated in PDMS (the microchannel is filled with dye for visualization). The outlets are numbered 1–8, starting from the inner channel wall. (*b*) SEM image illustrating the outlet section of the spiral microchannel.

Particle separation

In this work, the particle size dependence of the ratio of F_L and F_D in spiral microchannels was exploited to separate 10 µm, 15 µm, and 20 µm diameter particles. These particles were chosen because of their similarity in size with most cell samples. Before testing the particle mixture, particles were tested individually in channels of varying heights and *De*. For each channel height, *De* was increased by increasing the flow rate until a single focused particle stream formed at the outlet. Increasing the flow rate further, resulted in migration of the focused particle stream away from the channel inner wall towards the channel center. As the flow rate increased further, the Dean forces begin to dominate the inertial lift forces resulting in de-focusing of the particle stream. Similar behavior was also noted by Di Carlo *et al.* [36]. The equilibrium positions of the particle streams were recorded as a function of *De* and these results were used to select the optimum channel height and flow rate required to demonstrate multi-particle separation.

Figure 14(a) shows composite images indicating the position (x) of the 10 μm diameter particle streams as a function of De in microchannels of varying height (H = 90μm – 140 μm). The suspension of 10 μm diameter particles was introduced through both inlets and all images were captured in the 500 μm section just prior to the outlet. For a given channel height, the focused particle stream moved away from the channel wall at increasing De, indicating the dominance of the Dean force. Although an increase in flow velocity resulted in a greater lift force ($F_L \propto U_f^2$) as compared to the Dean drag ($F_D \propto U_f^{1.63}$), the stream movement away from the wall may be explained by decrease in the lift coefficient with increasing fluid flow velocity [44]. Hence, the net lift force reduced with increasing fluid flow velocity and the particle stream moved away from the channel wall. Increasing the channel height also resulted in focusing of particle streams further away from the channel inner wall, which may be explained by the fact that for a given flow velocity U_f the Dean drag force increases with channel height, while the lift force decreases with increasing channel height. Thus, the particle stream position can be altered by either increasing the De or increasing the channel height.

Figure 14(b) contains the corresponding graph showing the position of the 10 μm diameter particle streams inside microchannels of different height as a function of De. For a 10 μm diameter particle in a 90 μm high channel ($a_p/H \sim 0.11$), the distance of the particle stream from the wall remained constant up to De = 8.8 before rising linearly. The lift force acting on the particle below De = 8.8 was very much greater than F_D and hence the particle stream was unaffected by an increase in the fluid velocity. However, beyond a critical De (flow rate), F_D increases to the same order as F_L and hence the particle stream position varied linearly with the flow rate indicating a dominance of Dean drag. Increasing microchannel height reduced the critical De required for particle stream migration, as seen in Figure 14(b), due to a larger Dean

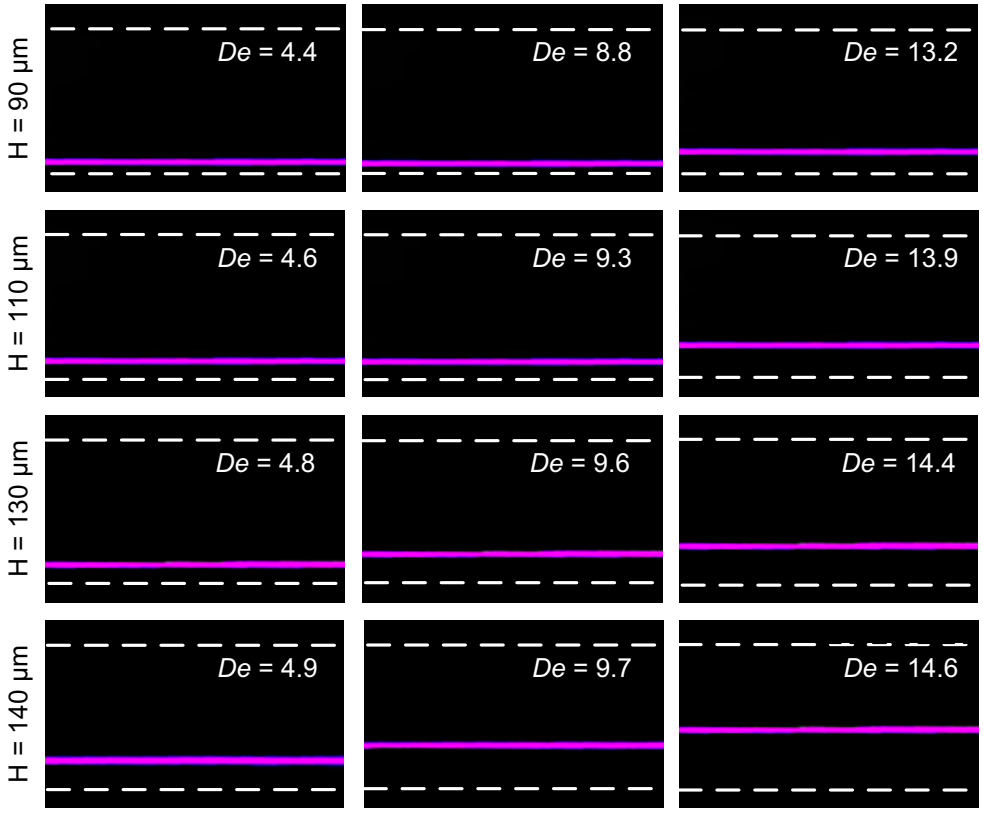

(a)

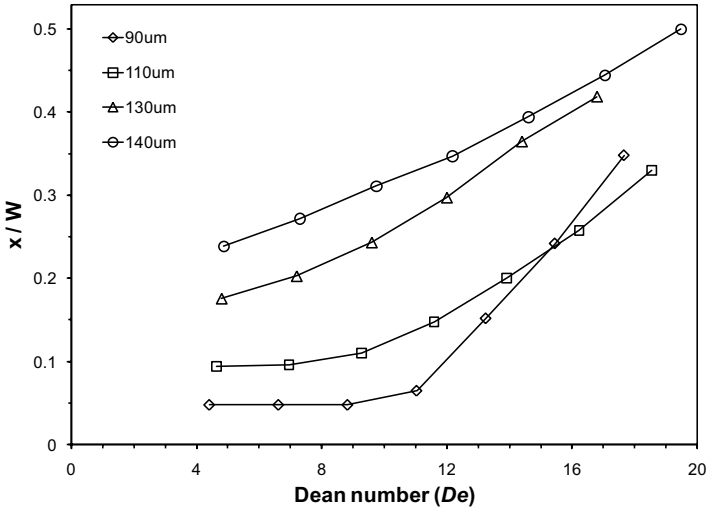

(b)

Figure 14. (a) Fluorescent images (pseudo-colored purple) illustrating the position of focused 10 µm diameter particle stream in spiral microchannels of different heights and at varying *De.* (b) Plots illustrating position of the 10 µm diameter particle streams from the inner channel wall for various *De* in microchannels ranging from 90 µm to 140 µm in height.

force with increase in channel height. Hence, in the case of 130 μm and 140 μm high channels ($a_p/H \sim 0.07$), the particle stream position varied for all flow conditions tested. For the larger 15 μm diameter particles (Figure 15), the higher a_p/H ratio in the case of the 90 μm and 110 μm microchannels resulted in a larger lift force and hence the particle stream positions remained predominantly constant for increasing *De*. However, similar to the 10μm diameter particles, an increase in channel height resulted in a lower $a_p/H \sim 0.1$ ratio and hence the position of the particle stream was strongly influenced by the Dean force.

The high a_p/H ratio of the 20 μm diameter particles resulted in a significant F_L acting on particles in each of the channel heights considered. Hence, a prominent flat (constant position) region is observed in all plots for the 20 μm diameter particles (Figure 16). The increased dominance of the lift force in the case of the larger particles is primarily due to the strong dependence of the lift force on the particle diameter ($F_L \propto a_p^4$ vs. $F_D \propto a_p$). Thus, in the 90 μm channel, the 20 μm diameter particle stream position was constant for almost all flow rates tested. Here again, an increase in channel heights resulted in significant particle migration away from the channel wall at higher flow rates.

Results from the individual particle tests indicate that a *complete* separation between the three particle sizes can be achieved in microchannels of different heights and a range of flow conditions. However in this particular case, it was found that the separation between the three particle streams was greatest in a 130 μm high channel. Thus, in the next set of experiments a homogenous mixture of 10 μm, 15 μm, and 20 μm diameter polystyrene particles labeled with DAPI, FITC and TRITC fluorophores was run through a 130 μm high spiral microchannel at *De* = 14.4 (flow rate ~ 3 mL/min).

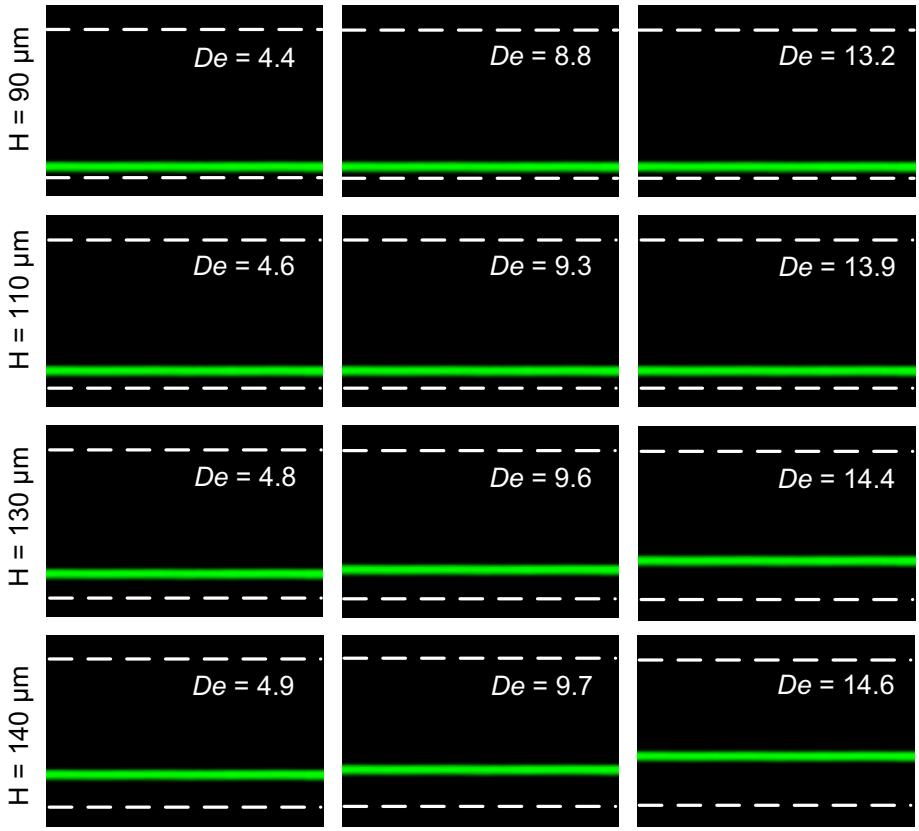

(a)

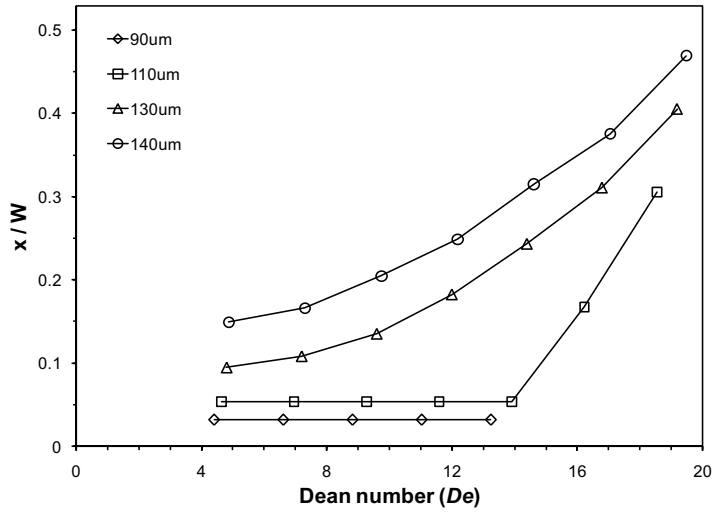

(b)

Figure 15. (a) Fluorescent images (pseudo-colored green) illustrating the position of focused 15 µm diameter particle stream in spiral microchannels of different heights and at varying *De.* (b) Plots illustrating position of the 15 µm diameter particle streams from the inner channel wall for various *De* in microchannels ranging from 90 µm to 140 µm in height.

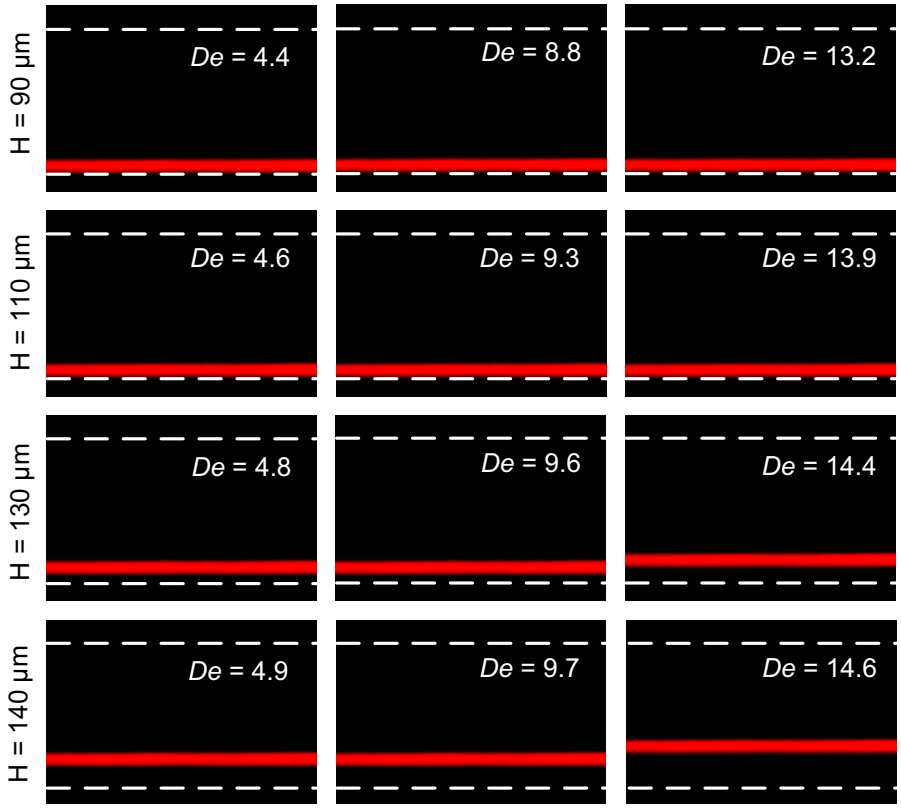

(a)

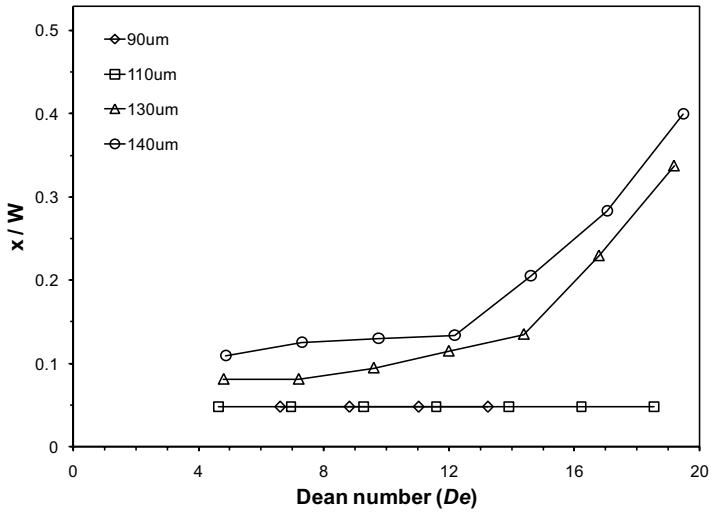

(b)

Figure 16. (a) Fluorescent images (pseudo-colored orange) illustrating the position of focused 20 µm diameter particle stream in spiral microchannels of different heights and at varying *De.* (b) Plots illustrating position of the 20 µm diameter particle streams from the inner channel wall for various *De* in microchannels ranging from 90 µm to 140 µm in height.

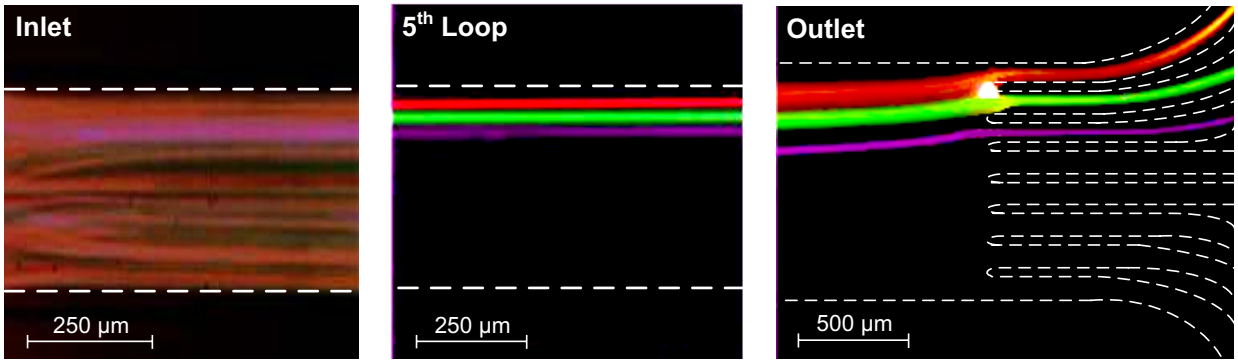

Figure 17. Superimposed fluorescent images illustrating distribution and position of the 20 µm (pseudo-colored orange), 15 µm, (pseudo-colored green), and 10 µm (pseudo-colored purple) diameter particles. The panels represent the inlet, a 500 µm wide channel section just prior to the outlet, and the bifurcated outlet of the 130 µm high spiral microchannel at De = 14.4. The randomly distributed particles at the inlet form ordered focused streams which are then collected separately at outlets 1, 2 and 3.

Multiple stream formation and particle separation was experimentally observed by using an epi-fluorescent microscope and corresponding filter cubes were used to capture images of each of the three particles at the channel outlet. Figure 17 shows the composite images of the created by superimposing the images captured from individual filter cubes. As mentioned previously, the 500 µm wide channel was opened into a 1 mm wide section at the outlet to achieve better separation by taking advantage of the laminar nature of microchannel flows. The composite images of the fifth loop and outlet sections in Figure 17 clearly indicate an increase in the separation between the three streams in the 1mm wide section of the channel. The position of the 10 µm, 15 µm, and 20 µm diameter particle streams in the 500 µm wide section of the channel were 180 µm, 120 µm, and 65 µm respectively from the inner microchannel wall. Thus, the three particles were collected at the first outlet, second outlet, and third outlets respectively. Although the channel height determines whether the particles focus into a single stream, it is the microchannel width that greatly influences the spacing between individual particle streams. Wider channels result in larger spacing between particle streams, which in turn permits

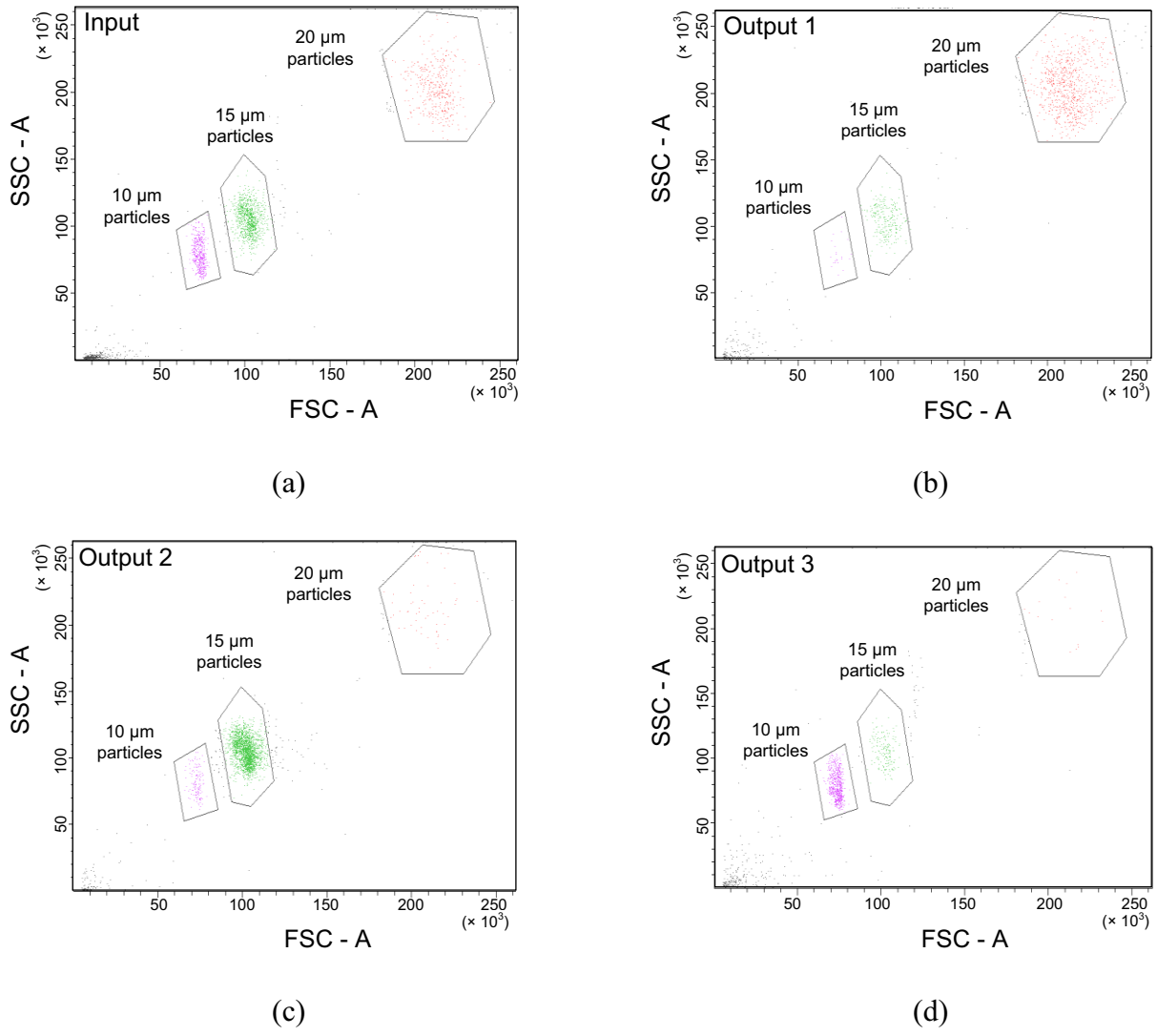

Figure 18. Flow cytometry data indicating concentration of the three particle mixture. The dot plots indicate concentration of the 10 µm, 15 µm, and 20 µm diameter particles at (*a*) the inlet, and (*b*-*d*) the first three outlets of the spiral channel. The gates in the side scatter vs. forward scatter panels were drawn using pure particle samples in order to discriminate between the three particle sizes.

separation of particles with smaller differences in diameter. Thus, the microchannel width influences the resolving capability of this separation technique.

The particle streams from each of the eight outlets were collected in separate vials and a flow cytometry analysis was performed to quantify the separation efficiency. Figure 18 presents the cytometry data (FSC Vs SSC) indicating the particle concentration at the inlet and the first three outlets of the spiral microchannel. Nearly 98% of the particles were filtered out at outlets 1, 2 and 3 (the outlets are numbered from the inner wall) suggesting a high degree of particle focusing. The scatter plots of output 1, 2, and 3 clearly show a very high concentration of 20 μm, 15 μm , and 10 μm diameter particles respectively.

Figure 19 illustrates distribution of each of the three particles across the eight outlets of the spiral microchannel. Since the absolute particle count cannot be obtained using the flow cytometry analysis, the obtained particle counts were normalized with respect to the inlet concentration for each of the three particles. The separation efficiency was calculated to be ~90% for the 20 μm diameter particles collected at outlet 1. The separation efficiency of the 15 μm and 10 μm diameter particles collected at outlets 2 and 3, respectively, was calculated to be in excess of 80%. By comparison, the separation efficiencies obtained using PFF and DLD, two active microfluidic techniques commonly used for particle separations, have been reported to be >90% [30-33].

The apparent lower separation efficiency of this passive microfluidic approach, however, is mainly attributed to the variation in individual particle sizes. In particular, the separation efficiency of the developed spiral system reduced to ~70% in the case of 20 μm diameter particles with a wider size distribution (σ = 2.5 μm), clearly indicating the dependence

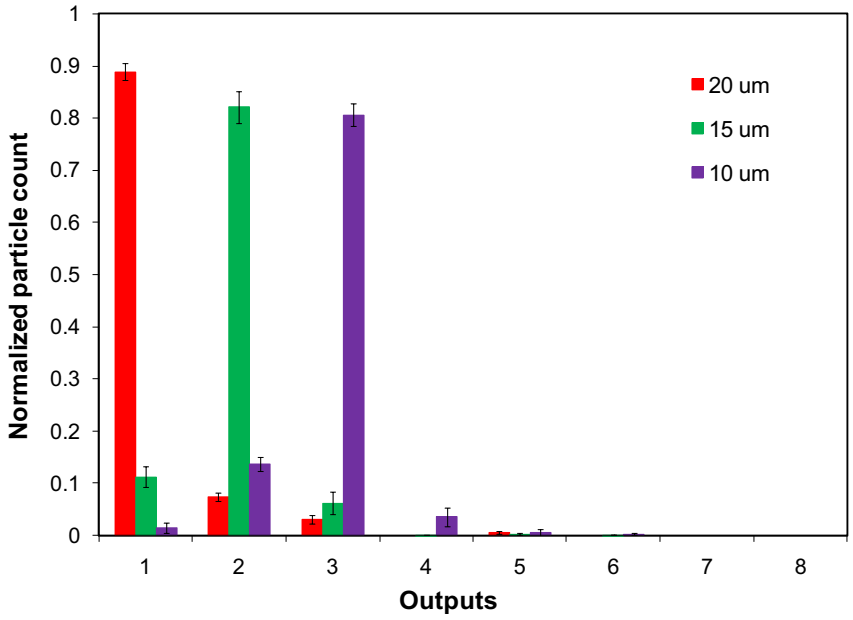

Figure 19. Flow cytometry results illustrating the distribution of the three particle sizes across the eight outlets of the spiral microchannel. The result clearly demonstrates ~85% separation efficiency between the three particle sizes.

of separation efficiency on particle size distribution. The separation efficiency can also be enhanced by designing wider spiral microchannels to increase spacing between the focused particles streams. Although, only separation of three particles sizes has been demonstrated in this work, a larger number of particle sizes can be simultaneously separated by using wider spiral microchannels.

Cell separation

Application of the developed technique to high-throughput cell sorting was demonstrated by using a spiral microchannel with appropriate dimensions to separate SH-SY5Y neuroblastoma and C6 glioma cells. Complete separation of these neural stem cells is of critical importance to understanding the specific and unique functions these cells play in the central nervous system (CNS), and potential applications in cell replacement therapy in many neurodegenerative

disorders (such as Parkinson's, Alzheimer's, or Multiple sclerosis) and cancer [13]. Based on the observed cell sizes, a homogenous mixture of the two cells was passed through a 120 μm high spiral microchannel at *De* = 11.8 (flow rate ~ 2.5 mL/min). The SH-SY5Y neuroblastoma cells which had an average diameter of ~15 μm were collected at outlet 1 and the smaller C6 glioma cells which had an average diameter of ~8 μm were collected at outlet 2. Figure 20 (a) shows the bright-field and epifluorescent images illustrating the distribution of the bigger SH-SY5Y cells (fluorescently labeled) and the smaller C6 glioma cells (unlabeled) at the inlet and at the first two outlets of the spiral microchannel. The inlet solution consisted of the two cell mixture with equal cell concentrations (~500,000 × 2 cells/mL). As expected, nearly 90% of the cells were filtered out at outlets 1 and 2 suggesting that the cells behave in the same way as the polystyrene beads. The cell counting data shown in Figure 20 (b) clearly indicates that the separation efficiency was >80% for both the bigger SH-SY5Y cells at outlet 1 and the smaller C6 glioma cells at outlet 2. The cell separation efficiency was limited by the large variations in the cell sizes (σ = 5 μm).

As Pamme [19] indicated in a recent review, continuous flow separation techniques are becoming popular on the microscale due to their ability to achieve very high sample throughputs. In spiral separators, since the inertial and Dean drag forces acting on the particles increase with increasing flow rates, the developed microparticle separator technique is ideal for achieving high throughput separations. For the flow rates tested, a sorting rate of 1 million cells/min (volume fraction 0.05%) was achieved using the spiral microparticle separator. The achieved throughput is significantly higher than the sorting rates of many microfluidic based cell sorting systems reported to date. For example, Fu *et al*. [52] demonstrated a throughput of ~7,000 cells/min (volume fraction 0.1%) while separating fluorescent and non-fluorescent *E. coli* cells in

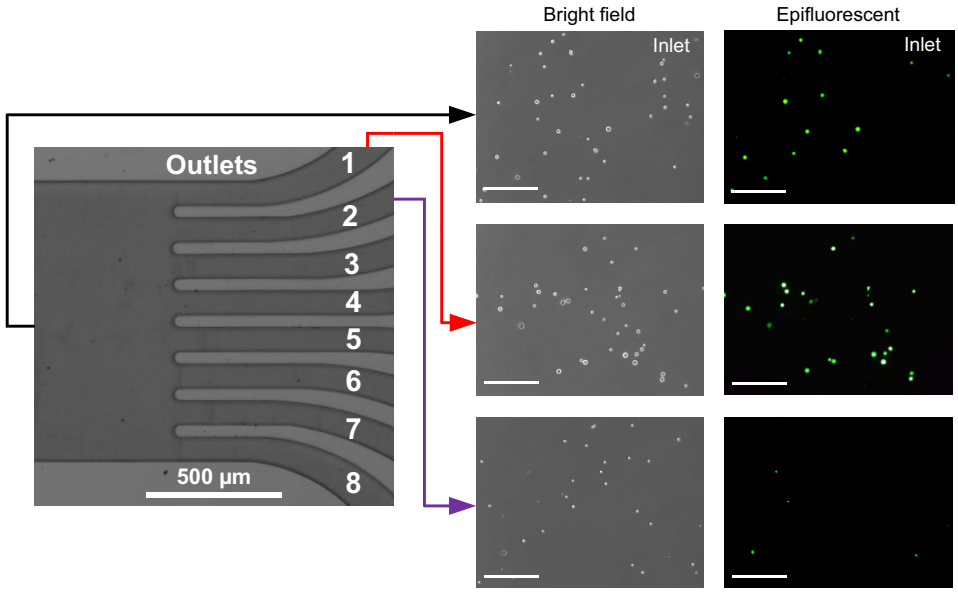

(a)

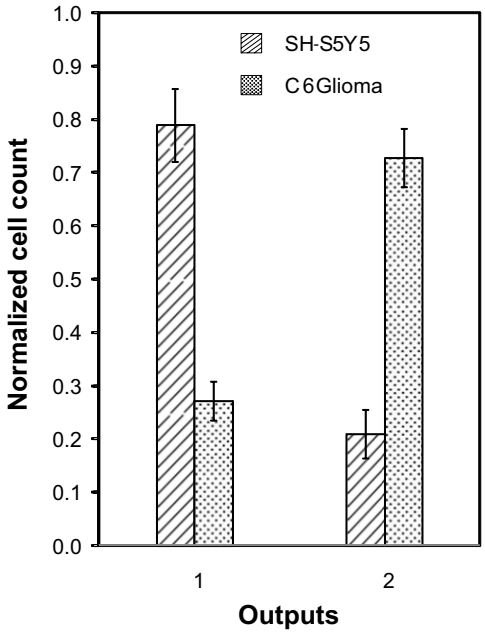

(b)

Figure 20. *(a)* Bright-field and epifluorescent images illustrating the distribution of the bigger ~15 µm diameter SH-SY5Y cells (pseudo-colored green) and the smaller ~8 µm diameter C6 glioma cells at the inlet and the first two outlets of the spiral microchannel (scale bar 100 µm). *(b)* Cell counting results clearly indicating ~80% separation efficiency between the two cells types, with the SH-SY5Y cells collected at outlet 1 and the C6 glioma cells at outlet 2.

microfluidic channels using fluorescently activated sorting technique. Recently, using PFF based cell separation Takagi *et al*. [53] demonstrated the separation of erythrocytes from diluted blood sample (volume fraction 0.3%) at a throughput of ~5,400 cells/min. The average throughput of many previously reported microfluidic sorting systems is ~2,000 cells/min [19]. Thus, the developed spiral system achieves > 100× higher throughput compared to other microscale sorting methods. Additionally, the throughput achieved is also comparable to the sorting rates obtained with commercial flow cytomerty techniques which have a maximum throughput of ~2.4 million cells/min [54]. The reported throughput may be further increased by increasing the cell volume fraction and fluid flow rates. Finally, a concern when working with such high flow rates is the potential irreversible damage to the cells due to the high shear forces. The cell viability following separation was confirmed by bringing both SH-SY5Y neuroblastoma and C6 glioma cells back into culture using the procedure described in the methods section with >90% cell recovery.

CHAPTER 5

CONCLUSIONS

Microparticle separators are integral components of most LOC devices developed for biological and environmental applications. In the recent years, several passive and active particle separation techniques have been reported. In particular, passive separation techniques have gained popularity because of their numerous advantages such as simpler design, ease of integration, high throughput. However, most passive microparticle separation techniques reported to date suffer from critical disadvantages including the inability to separate multiple particles quickly and efficiently and the inability to simultaneously separate wide range of particle sizes. Hence, there is a need to develop a high throughput, multi-particle separator capable of operating over a wide range of particle sizes.

This work reported a Dean coupled inertial microfluidic system for passive and simultaneous separation of microparticle mixtures. Particles flowing through a spiral microchannel are subject to both Dean drag and inertial lift forces. The ratio of the inertial lift to Dean drag forces acting on the particle is dependent of the diameter of the particle. The particle size dependence of the ratio of forces was exploited to generate focused streams of individual particles at distinct positions within the microchannels cross-section. Initially, individual particles were tested in spiral microchannels with heights ranging from 90 μm to 140 μm to identify the various design parameters influencing the particle position. Channel cross-sectional

dimension, fluid flow velocity, channel length and finally the outlet design were identified to be the key parameters influencing particle separation efficiency. Based on the above parameters, a 40 cm long spiral microchannel with a cross-sectional dimension of 500 μm × 130 μm was designed and fabricated. The 500 μm wide channel section was opened up into a 1 mm wide segment to increase spacing between particle streams before splitting into eight 100 μm wide outlets. With an input fluid velocity of ~ 3 mL/min, a mixture of 10 μm, 15 μm, and 20 μm diameter particles were separated with separation efficiency of ~85%. The device was also used to show a high throughput (1 million cells/min) separation of SH-SY5Y neuroblastoma and C6 glioma cells, demonstrating a possible application of this technique in microscale cell sorting.

Thus, the key impact of this work is that it demonstrates a technique to passively and continuously separate multi-particle mixture in a single run. The passive nature of the separation principle and the planar nature of the described design will permit easy integration with existing LOC systems requiring high-throughput separations.

The results in this thesis demonstrate the feasibility of simultaneously separating microparticles based on their size using the principle of Dean coupled inertial migration. However, the exact theory behind particle separation is not yet fully understood. Hence, future work could focus on obtaining a better understanding of the forces affecting particle motion and thus developing an analytical model to theoretically predict the final equilibrium position of the particle for a give set of flow conditions. Specifically, it is important to address the following issues:

1) *Lift Coefficient:* Lift coefficient and hence the lift force acting on a particle depends on the position of the particle and *Re*. Since the particle position is influenced by the ratio of

the inertial lift to Dean drag forces, an accurate evaluation of the lift forces acting on the particle will greatly help in predicting the final equilibrium position of the particle.

2) *Computational Model:* The complex three dimensional nature of the problem necessitates the need to develop a computational model to fully and better understand the various forces acting on the particle. Since the particle sizes in this work are comparable to the channel dimension, the macroparticle module can be employed to obtain accurate results.
3) *Outlet Design:* In this work the separation between the particle streams in the 500 μm section of the channel was increased by opening up the 500 μm section in to a 1mm wide section. By opening up the channel in to a much wider section and designing suitable outlets the separation efficiency of this device can be further improved. Additionally, it was also observed that the pressure drop across individual outlet channels, greatly affected the collection efficiency (collecting the separated streams). Thus, by designing an outlet system with equal pressure drop across all the outlets, the separation efficiency can be further improved.

REFERENCES

[1] M. Toner and D. Irimia, "Blood-on-a-chip," *Annu. Rev. Biomed. Eng.*, vol. 7, pp. 77-103, 2005.

[2] G. Blankenstein and U. D. Larsen, "Modular concept of a laboratory on a chip for chemical and biochemical analysis," *Biosens. Bioelect.*, vol. 13, pp. 427-438, 1998.

[3] J. West, M. Becker, S. Tombrink, and A. Manz, "Micro Total Analysis Systems: Latest Achievements," *Anal. Chem*, vol. 80, pp. 4403-4419, 2008.

[4] G. M. Whitesides, "The origins and the future of microfluidics," *Nature*, vol. 442, pp. 368–373, 2006.

[5] P. Yager, T. Edwards, E. Fu, K. Helton, K. Nelson, M. R. Tam and B. H. Weigl, "Microfluidic diagnostic technologies for global public health," *Nature*, vol. 442, pp. 412-418, 2006.

[6] J.Knight, "Honey, I shrunk the lab," *Nature*, vol. 418, pp. 474-475, 2002.

[7] M. Freemantle, "Downsizing chemistry," *Chem. and Engg. News*, vol. 8, pp. 27-36, Feb.1999.

[8] S. Borman, "Microchips deliver on command," *Chem. and Engg. News*, vol. 5, pp. 30-31, Feb. 1999.

[9] J. Khandurina, T. E McKnight, S. C. Jacobson, L. C. Waters, R. S. Foote, and J. M. Ramsey, "Integrated system for rapid PCR-based DNA analysis in microfluidic devices," *Anal. Chem*., vol. 72, pp. 2995-3000, 2000.

[10] M. Kopp, A. D. Mello, and A. Manz, "Chemical amplification: continuous-flow PCR on a chip," *Science*, vol. 280, pp. 1046-1048, 1998.

[11] P. Belgrader, M. Okuzumi, F. Pourahmadi, D. A. Borkholder, and M. A. Northrup, "A microfluidic cartridge to prepare spores for PCR analysis," *Biosens. Bioelectron.*, vol. 14, pp. 849-852, 2000.

[12] I. K Glasgow, H. C. Zeringe, D. J. Beebe, S. J Choi, J. T. Lyman, N. G. Chan, and M. B. Wheeler, "Handling individual mammalian embryos using microfluidics," *IEEE Trans. Biomed. Engg.*, vol. 48, pp. 570-578, 2001.

[13] Z. Wu, K. Hjort, G. Wicher and A. Fex Svenningsen, "Microfluidic high viability neural cell separation using viscoelastically tuned hydrodynamic spreading," *Biomed. Microdevices*, vol. 10, pp. 631-638, 2008

[14] I. Kheterpal, and R. A. Mathies, "Capillary array electrophoresis DNA sequencing," *Anal.Chem*., vol. 71, pp. 31A-37A, 1999.

[15] D. J. Harrison, K. Fluri, K. Seiler, Z. Fan, C. S. Effenhauser, and A. Manz, "Micromachining a miniaturized capillary electrophoresis-based chemical analysis system on a chip," *Science*, vol. 261, pp. 895-897, 1993.

[16] S. B. Cheng, C. D. Skinner, J. Taylor, S. Attiya, W. E. Lee, G. Picelli, and J. D. Harrison, "Development of a multichannel micro fluidic analysis system employing affinity capillary electrophoresis for immunoassay," *Anal. Chem*., vol.73, pp. 1472-1479, 2001.

[17] L.C. Waters, S. C. Jacobson, N. Kroutchinina, J. Khandurina, R. S. Foote, and M. J. Ramsey, "Microchip device for cell lysis, multiplex PCR amplification and electrophoretic sizing," *Anal. Chem*., vol. 70, pp. 158-162, 1998.

[18] M. Kersaudy-Kerhoas, R. Dhariwal, and M.P.Y. Desmulliez, "Recent advances in microparticle continuous separation," *IET Nanobiotechnol.*, vol. 2, pp. 1-13, 2008.

[19] N. Pamme, "Continuous flow separations in microfluidic devices," *Lab Chip*, vol. 7, pp. 1644-1659, 2007.

[20] X. Xu, K.K. Caswell, E. Tucker, S. Kabisatpathy, K. L. Brodhacker, and W. A. Scrivens, "Size and shape separation of gold nanoparticles with preparative gel electrophoresis," *J. Chromatogr., A*, vol. 1167, pp. 35–41, 2007.

[21] L.J. Yang, P.P. Banada, M.R. Chatni, K. S. Lim, A. K. Bhunia, M. Ladisch and Rashid Bashir, "A multifunctional micro-fluidic system for dielectrophoretic concentration coupled with immuno-capture of low numbers of Listeria monocytogenes," *Lab Chip*, vol. 6, pp. 896–905, 2006.

[22] N. Pamme and A. Manz, "On-chip free-flow magnetophoresis: continuous flow separation of magnetic particles and agglomerates," *Anal. Chem.*, vol. 76, pp. 7250–7256, 2004.

[23] T. Deng, M. Prentiss and G.M. Whitesides, "Fabrication of magnetic microfiltration systems using soft lithography," *Appl. Phys. Lett.*, vol. 80, pp. 461-463, 2002.

[24] C. W. Yung, J. Fiering, A. J. Mueller and D. E. Ingber, "Micromagnetic–microfluidic blood cleansing device," *Lab Chip.*, vol. 9, pp. 1171-1177, 2009

[25] M.P. Macdonald, G.C. Spalding, and K. Dholakia, "Microfluidic sorting in an optical lattice," *Nature*, vol. 426, pp. 421–424, 2003.

[26] K. Ladavac,K. Kasza, and D.G. Grier, "Sorting mesoscopic objects with periodic potential landscapes: Optical fractionation," *Phys. Rev. E*, vol. 70, p. 01090, 2004.

[27] J.P. Brody and P. Yager, "Diffusion-based extraction in a microfabricated device," *Sens. Actuators, A*, vol. 58, pp. 13-18, 1997.

[28] P. Jandik, B. H. Weigl, N. Kessler, J. Cheng, C. J. Morris, T. Schulte and N. Avdalovic, "Initial study of using a laminar fluid diffusion interface for sample preparation in high-performance liquid chromatography," *J. Chromatogr., A*, vol. 954, pp. 33–40, 2002.

[29] M. Yamada, M. Nakashima and M. Seki, "Pinched flow fractionation: continuous size separation of particles utilizing a laminar flow profile in a pinched microchannel," *Anal. Chem.*, vol. 76, 5465-5471, 2004.

[30] L. R. Huang, E. C. Cox, R. H. Austin and J. C. Sturm, "Continuous particle separation through deterministic lateral displacement," *Science*, vol. 304, pp. 987–990, 2004.

[31] D. W. Inglis, J. A. Davis, R. H. Austin and J. C. Sturm, "Critical particle size for fractionation by deterministic lateral displacement," *Lab Chip.*, vol. 6, pp. 655-658, 2006

[32] P. Beech and J. O. Tegenfeldt, "Tuneable separation in elastomeric microfluidics devices," *Lab Chip*, vol. 8, pp. 657-659, 2008.

[33] E. Chmela, R. Tijssen, M. T. Blom, H. J. G. E. Gardeniers and A. van den Berg, "A chip system for size separation of macromolecules and particles by hydrodynamic chromatography," *Anal. Chem.*, vol. 74, pp. 3470 – 3475, 2002.

[34] M. T. Blom, E. Chmela, R. E. Oosterbroek, R. Tijssen and A. van den Berg, "On-chip hydrodynamic chromatography separation and detection of nanoparticles and biomolecules," *Anal. Chem.,* vol. 75, pp. 6761 – 6768, 2003.

[35] A. A. S. Bhagat, S. S. Kuntaegowdanahalli and I. Papautsky, "Enhanced particle filtration in straight microchannels using shear-modulated inertial migration," *Phys. Fluids*, vol. 20, pp. 101702, 2008.

[36] D. Di Carlo, D. Irimia, R. G. Tompkins and M. Toner, "Continuous inertial focusing, ordering, and separation of particles in microchannels," *PNAS*, vol. 104, pp. 18892-18897, 2007.

[37] D. Di Carlo, J. F. Edd, D. Irimia, R. G. Tompkins and M. Toner, "Equilibrium separation and filtration of particles using differential inertial focusing," *Anal. Chem.*, vol. 80, pp. 2204-2211, 2008.

[38] A. A. S. Bhagat, S. S. Kuntaegowdanahalli and I. Papautsky, "Continuous particles separation in spiral microchannels using Dean flows and inertial migration," *Lab Chip*, vol. 8, pp. 1906-1914, 2008.

[39] W. R. Dean, "Note on the motion of fluid in a curved pipe," *Phil. Mag. Ser.,* vol. 4, pp. 208–223, 1927.

[40] W. R. Dean, "The streamline motion of fluid in a curved pipe," *Phil. Mag. Ser.*, vol. 5, pp. 673–695, 1928.

[41] S. Ookawara, R. Higashi, D. Street and K. Ogawa, "Feasibility study on concentration of slurry and classification of contained particles by microchannel," *Chem. Eng. J.*, vol. 101, pp. 171-178, 2004.

[42] S. Ookawara, D. Street and K. Ogawa, "Numerical study on development of particle concentration profiles in a curved microchannel," *Chem. Eng. Sci.*, vol. 61, pp. 3714-3724, 2006.

[43] R. Eichhorn and S. Small, "Experiments on the lift and drag of spheres suspended in a Poiseuille flow," *J. Fluid Mech.*, vol. 20, pp. 513-527, 1964.

[44] E. S. Asmolov, "The inertial lift on a spherical particle in a plane Poiseuille flow at large channel Reynolds number," *J. Fluid Mech.*, vol. 381, pp. 63-87, 1999.

[45] G. Segre and A. Silberberg, "Behaviour of macroscopic rigid spheres in Poiseuille flow Part 2. Experimental results and interpretation," *J. Fluid Mech.*, vol. 14, pp. 136-157, 1962.

[46] G. Segre and A. Silberberg, "Radial particle displacements in Poiseuille flow of suspensions," *Nature*, vol. 189, pp. 209-210, 1961.

[47] B. Chun and A. J. C. Ladd, "Inertial migration of neutrally buoyant particles in a square duct: An investigation of multiple equilibrium positions," *Phys. Fluids*, vol. 18, p. 031704, 2006.

[48] I. Gregoratto, C. J. McNeil and M. W. Reeks, "Micro-devices for rapid continuous separation of suspensions for use in micro-total-analysis-systems," *Proc. SPIE*, vol. 6465, p. 646503, 2007.

[49] J. Seo, M. H. Lean and A. Kole, "Membrane-free microfiltration by asymmetric inertial migration," *Appl. Phys. Lett.*, vol. 91, pp. 033901, 2007.

[50] J. Seo, M. H. Lean and A. Kole, "Membraneless microseparation by asymmetry in curvilinear laminar flows," *J. Chromatogr. A*, vol. 1162, pp. 126-131, 2007.

[51] A. A. S. Bhagat, E. T. K. Peterson, and I. Papautsky, "A passive planar micromixer with obstructions for mixing at low Reynolds numbers," *J. Micromech. Microeng*., vol. 17, pp. 1017-1024, 2007.

[52] A. Y. Fu, C. Spence, A. Scherer, F. H. Arnold, and S. R. Quake, "A Microfabricated Fluorescence-Activated Cell Sorter," *Nature Biotech.*, 1999, **17**, 1109-1111.

[53] J. Takagi, M. Yamada, M. Yasuda and M. Seki, "Continuous particle separation in a microchannel having asymmetrically arranged multiple branches," *Lab Chip*, 2005, **5**, 778-784.

[54] T. D. Chung and H. C. Kim, "Recent advances in miniaturized microfluidic flow cytometry for clinical use," *Electrophoresis*, vol 28, pp. 4511-4520, 2007.